Transonic Pressure, Force, and Flow-Visualization Measurements on a Pitching Straked Delta Wing at High Alpha

Atlee M. Cunningham, Jr.
Lockheed Martin Aeronautics Company
P. O. Box 748, MZ 2828
Fort Worth, Texas, TX 76 101, United States

Evert G.M. Geurts
National Aerospace Laboratory (NLR)
Anthony Fokkerweg 2
1059 CM Amsterdam
The Netherlands

SUMMARY

A force and pressure test was conducted in May 1992 (at the National Aerospace Laboratory [NLR], The Netherlands) on a simple straked wing with the objective to extend the understanding of flow fields at low speed and high incidence obtained in earlier tests, up to transonic speeds also at high incidences. A flow-visualization test was then conducted with the same simple straked wing modes in August 1996 for the purpose of obtaining flow-visualization data to complement the pressure and force database generated in the earlier tests. These tests were conducted in order to examine the flow-field characteristics at high-alpha conditions that involve vortices, shocks, and separated flows. Laser light sheet/water vapor techniques were used to illuminate the flows, and video recording was used to obtain the data. Both low- and high-speed video cameras were used to examine spanwise and streamwise laser sheet positions. In addition, under NLR funding, some preliminary particle image velocimetry (PIV) data were obtained at M = 0.225 and 0.6, as well as some pulsed laser-flow visualization (9 nano-sec pulse) at M = 0.9. Correlation was performed between the flow-visualization data from this test and the pressure/force data obtained in 1992 on the same configuration. The database described in this paper has been included in the RTO database for verification and validation data for computational unsteady aerodynamics.

NOMENCLATURE

C_m	=	wing pitching-moment coefficient	M,MACH	=	freestream Mach number
C_N	=	wing normal-force coefficient	p	=	pressure at model surfaces
C_p	=	pressure coefficient	p_s	=	freestream static pressure
	=	$(p - p_s)/Q$	Q	=	dynamic pressure
C_r	=	reference chord, 0.821 m	α	=	angle-of-attack, deg

1.0 INTRODUCTION

Steady and unsteady low-speed wind tunnel tests were conducted in 1986 on a pitching simple straked wing model representative of modern fighter aircraft, which make use of a strake/wing combination to achieve good, high angle-of-attack aerodynamic characteristics (References 1 and 2). The model was oscillated in pitch at amplitudes sufficient to represent rapid pitch-ups and push-overs at dynamically scaled, full-scale maneuver times. Force and pressure data, as well as flow-visualization information, were obtained so that a better

Paper presented at the RTO AVT Symposium on "Advanced Flow Management: Part A – Vortex Flows and High Angle of Attack for Military Vehicles", held in Loen, Norway, 7-11 May 2001, and published in RTO-MP-069(I).

Report Documentation Page

Form Approved
OMB No. 0704-0188

1. REPORT DATE	2. REPORT TYPE	3. DATES COVERED
00 MAR 2003	**N/A**	**-**

4. TITLE AND SUBTITLE	5a. CONTRACT NUMBER
Transonic Pressure, Force, and Flow-Visualizataion Measurements on a Pitching Straked Delta Wing at High Alpha	5b. GRANT NUMBER
	5c. PROGRAM ELEMENT NUMBER
6. AUTHOR(S)	5d. PROJECT NUMBER
	5e. TASK NUMBER
	5f. WORK UNIT NUMBER
7. PERFORMING ORGANIZATION NAME(S) AND ADDRESS(ES) **NATO Research and Technology OrganisationBP 25, 7 Rue Ancelle, F-92201 Neuilly-Sue-Seine Cedex, France**	8. PERFORMING ORGANIZATION REPORT NUMBER
9. SPONSORING/MONITORING AGENCY NAME(S) AND ADDRESS(ES)	10. SPONSOR/MONITOR'S ACRONYM(S)
	11. SPONSOR/MONITOR'S REPORT NUMBER(S)

12. DISTRIBUTION/AVAILABILITY STATEMENT
Approved for public release, distribution unlimited

13. SUPPLEMENTARY NOTES
Also see: ADM001490, Presented at RTO Applied Vehicle Technology Panel (AVT) Symposium held inLeon, Norway on 7-11 May 2001, The original document contains color images.

14. ABSTRACT

15. SUBJECT TERMS

16. SECURITY CLASSIFICATION OF:			17. LIMITATION OF ABSTRACT	18. NUMBER OF PAGES	19a. NAME OF RESPONSIBLE PERSON
a. REPORT	b. ABSTRACT	c. THIS PAGE			
unclassified	**unclassified**	**unclassified**	**UU**	**28**	

Standard Form 298 (Rev. 8-98)
Prescribed by ANSI Std Z39-18

understanding of the developing flow fields associated with such maneuvers could be obtained. These extensive analyses, which have been documented in References 3 through 6, show how wing and strake vortices develop and interact, as well as how they break down and collapse to fully stalled flows.

The interest to extend this understanding to include compressibility effects led to the consideration of another test of a similar configuration at transonic speeds. Thus, plans were made to conduct a wind tunnel test to investigate unsteady pressures and forces for a simple straked wing under the same dynamical conditions tested at low speeds in 1986, but at increasing speeds up to the transonic regime. This planned test, as discussed in Reference 7, was accomplished in May 1992 for the simple straked wing test (Reference 8) and had the straightforward objective to simply extend the understanding of flow fields at low speeds and high incidences up to transonic speeds and high incidences.

Analyses of the force and pressure data from the simple straked wing (Reference 8) raised many questions concerning the nature of the flow fields involved. These questions were further augmented as a result of a preliminary flow-visualization investigation conducted on the simple straked wing at the conclusion of that test in May 1992 (Reference 9). The objectives of this test were to understand the physics or unsteady transonic flows at high-incidence conditions and to develop appropriate databases to be used for validating computational fluid dynamic codes for realistic flow phenomena. Thus, further flow-visualization testing was needed in order to answer the questions that were raised in Reference 8.

A flow-visualization test was conducted with the simple straked wing in August 1996 (at the NLR, The Netherlands), with the purpose of meeting the needs outlined above. This test was conducted to examine the flow-field characteristics at high-alpha conditions that involve vortices, shocks, and separated flows. Laser light sheet/water vapor techniques were used to illuminate the flows, and video recording was used to obtain the data. Both low- and high-speed video cameras were used to examine spanwise and streamwise laser sheet positions. In addition, under NLR funding, some preliminary particle image velocimetry (PIV) data were obtained at M = 0.225 and 0.6, as well as some pulsed laser-flow visualization (9 nano-sec pulse) at M = 0.9. Complete details of the test setup, procedures, data points, and database are given in the NLR test report (Reference 10). Test summary, presentation of pressure and flow-visualization data, and discussions of results are given in References 11, 12, and 13.

2.0 TEST SETUP AND PROCEDURES

The simple straked wing model used in the flow-visualization test in August 1996 was the same model used in the force/pressure test up to post-stall conditions at transonic speeds in May 1992 at NLR (Reference 8). The objective of the 1996 test was to obtain flow-visualization data that would complement the force and pressure data obtained in 1992. Thus, test conditions for the second test were driven by those of the first test.

A complete description of the NLR High-Speed Wind Tunnel (HST) in Amsterdam and its operation is given in Reference 10. Also included in Reference 10 are descriptions of the model, model support, model excitation (pitch oscillation), instrumentation, and flow-visualization setup. A description of the pulsed laser-flow visualization and PIV setup is included in Reference 14.

The force, pressure, and flow-visualization test was conducted in the NLR HST located in Amsterdam. The tunnel has a closed circuit with a test section length of about 2.5m. It was operated with a 2.0m x 1.6m test section, and sidewall mounting was used for the semi-span straked wing model. The tunnel has a Mach range of 0.3 to 1.2, and a maximum Reynolds number of 22 x 10^6 per meter at M = 0.95.

The model was the semi-span, simple straked wing configuration shown in Figure 1, which was supported on a semi-span balance that was driven by a hydraulic actuator mounted on a movable turntable. This arrangement permitted independent control of oscillatory pitching motion and model mean angle-of-attack. The model was instrumented with a main wing semi-span balance, dynamic incidence transducer, in situ pressure tranducers, and vertical accelerometers, all located as shown in Figure 1. The pressure transducers were taped over for the flow-visualization test and were not operative. The pressure rows, however, were used as reference positions

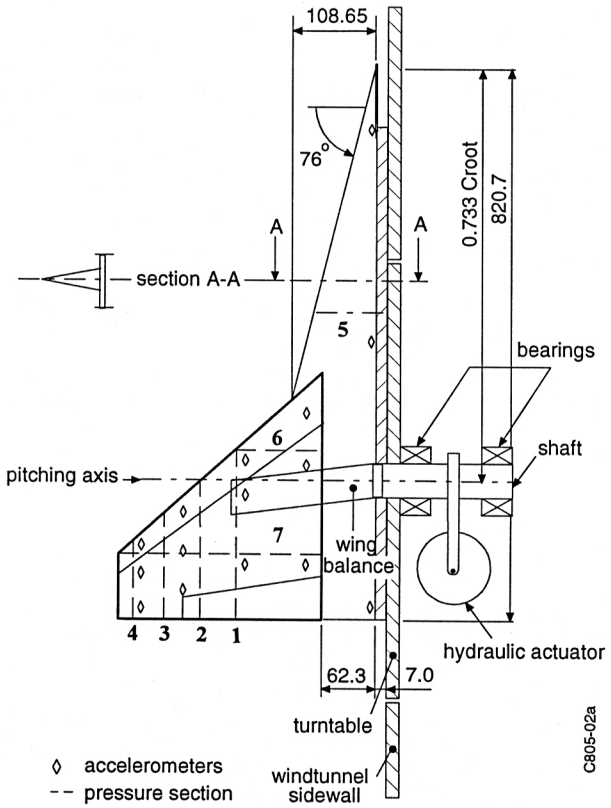

Figure 1: Semi-Span Straked Wing Model and Instrumentation

orientations; however, conventional video recording was accomplished from both downstream (sting camera) and side view directions, also shown in Figure 3. The high-speed video recordings were in a positive format of white vapor image on black background. However, negative image of the IHSV frames provided improved quality and contrast for use in this final report, as is shown in Figure 4.

The pulsed laser-flow visualization and PIV setup are shown in Figure 5 (Reference 14). Side view mounting for the high-resolution camera was used in order to conduct preliminary tests on making PIV measurements at high speeds. The pulsed laser was set at a single streamwise position (Number 3 in Figure 2), and all PIV and flow-visualization measurements were at this position. Seeding for PIV was accomplished at M = 0.225 and 0.6 by injecting oil smoke and nebulized oil into the settling chamber from a rake. At M = 0.9, flow visualization was accomplished with water vapor in the same manner as discussed above.

3.0 FORCE DATA AND FLOW-FIELD CHARACTERISTICS

A low-speed test of the full-span straked wing model was conducted at NLR in 1986 (References 1-6). This model was instrumented for force and unsteady pressure measurements. Incidences of from -8 deg up to 50 deg were for the laser light sheet locations. Numbering and locations of the light sheet positions are shown in Figure 2, where it will be noted that these numbers do not generally correspond to those for the pressure rows in Figure 1.

Flow visualization was accomplished by controlling humidity in the wind tunnel by spraying water downstream of the model into the tunnel, as needed, and varying the tunnel temperature and pressure during the test. This approach provided the proper conditions to produce water condensation only in the expansion regions above the model. Illumination of the water vapor was achieved with a 5-watt continuous argon laser whose beam was spread into a sheet with a cylindrical lens (see Figure 3). The sheet position and orientation were remotely controlled on a traversing system, which provided a coverage that exceeded the model dimensions. High-speed video recording with the Kodak Intensified High-Speed Video Camera (IHSV) was accomplished only for span-wise sheet

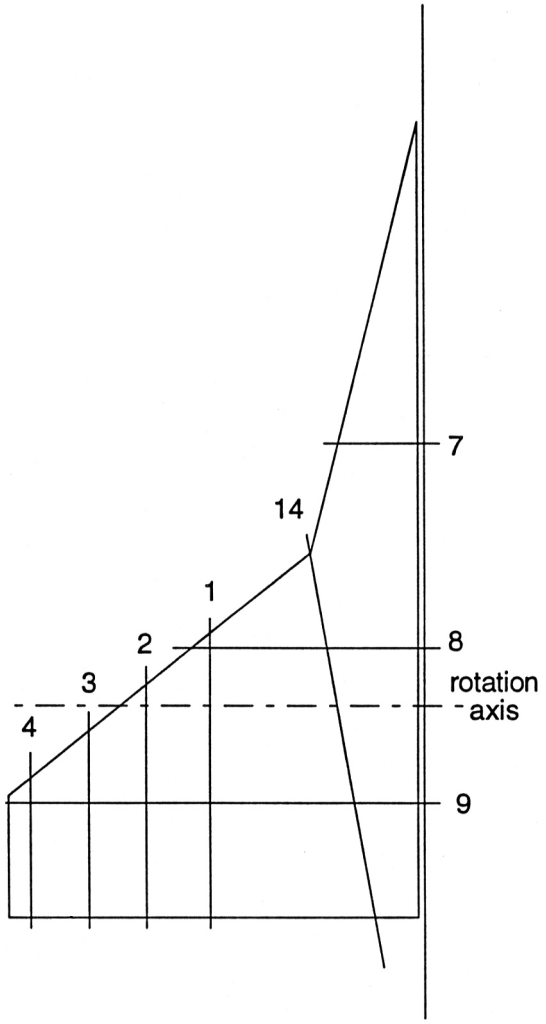

Figure 2: Laser Light Sheet Positions for Various Configurations

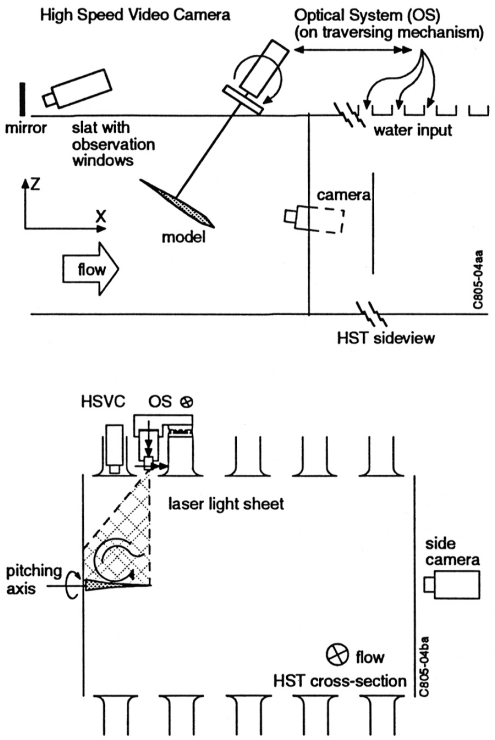

Figure 3: Vapor Screen Visualization Setup for High-Speed and Conventional Video Cameras in the HST

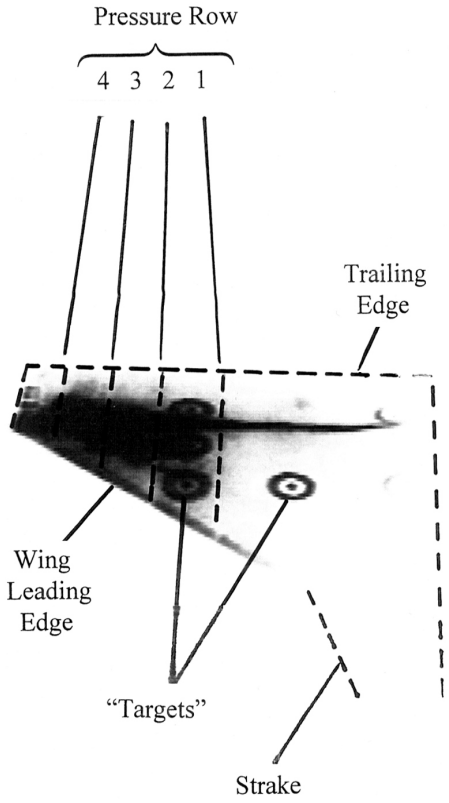

Figure 4: Negative High-Speed Video Frame Format

tested with the model, both stationary and oscillating in pitch at either 0 deg or ±5 deg sideslip. Amplitudes of oscillation ranged from ±2 deg to ±18 deg. The Mach number was constant at M = 0.225 with a Reynolds number of 3.7 x 10^6 based on the root chord.

The semi-span model tested in 1992 was shown in Reference 8 to correlate reasonably well with the full span model at M = 0.225 and a Reynolds number of 3.7 x 10^6. The semi-span model was tested at a higher Reynolds number of 8.0 x 10^6 for increasing Mach from 0.225 to 0.9. Even though the exact points for critical flow transitions did not completely match for the two models, the trends were very similar, indicating that the important flow mechanisms were preserved on the semi-span model.

Results for the semi-span model shown in Figure 6 for M = 0.225, 0.6, and 0.9 at a Reynolds number of 8 x 10^6 illustrate the transition from low speeds to transonic speeds. All three C_N curves are very similar with exception of (1) the higher slope at M = 0.9 and angles less than 10 deg, and (2) the higher peak at about 24 deg for M = 0.6. The C_m curves are also very similar, and show a typical aft movement of the center or pressure with increasing Mach. Based on analysis of pressure data, the flow-field characteristics at M = 0.6 are very similar to those at M = 0.225. The peak at

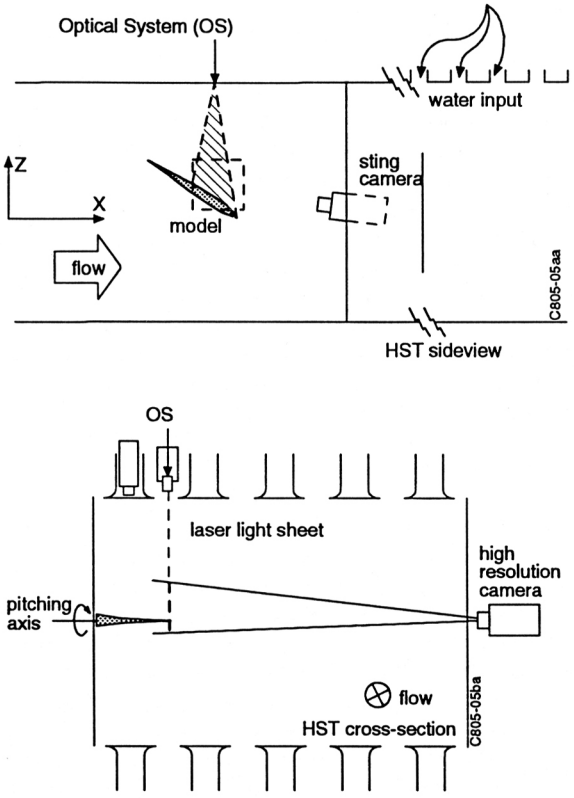

Figure 5: Particle Image Velocimetry Setup With the Pulsed Laser in the HST

about 24 deg in the M = 0.6 C_N curve is caused by a more severe process of vortex bursting where lift over most of the wing is affected. At M = 0.225, this process occurs more toward the trailing edge, and hence is not as noticeable. Although the C_N and C_m curves at M = 0.9 are similar to the others over much of the angle range, the flow characteristics are very different. The only common feature is the strake vortex.

In References 1-6, a description of flow-field development for the simple straked wing was presented in the form of C_L and C_m curves with various flow characteristics identified according to the incidence range of their occurrence. A similar version for transonic speeds is shown in Figure 7 for the semi-span wing in the high-speed test at M = 0.9. The trends up to about 10 deg represent essentially attached transonic flow developments, which are dominated by shocks on the 40 deg swept outer wing panel. With incidence increasing beyond 10 deg, the formation of shock-induced trailing edge separation (SITES) occurs at about 10.5 deg over the outer 20% of the wing. A further increase to above 11.0 deg results in the onset of leading edge separation, which is indicated at the three outboard streamwise pressure rows 2, 3, and 4 (see Figure 1). These two transitions result in a flat C_N slope and a pitch-up in C_m , as seen in Figure 7.

Above 11.0 deg, vortex flow development begins with the strake vortex. There does not appear to be a wing vortex analogous to that seen at lower speeds as postulated in References 8 and 9. Instead, the outer wing flows appear to be dominated by a mixture of leading edge separation, SITES, and forward shock development.

At around 18.5 deg, the outboard wing flow transitions to a new structure referred to as “finger vortices” and “shocklets” as was seen in the flow-visualization data (Reference 9). This transition also corresponds to the occurrence of maximum suction at the spanwise pressure row, Section 6 (see Figure 1). Development of this new flow continues up to about 27.0 deg and has a more forward lift location as indicated by a greater pitch-up trend in the C_m curve. The strake vortex continues to develop until at about 25.5 deg, bursting appears in the pressure data and in the flow-visualization data (Reference 9) at Section 7 (see Figure 1).

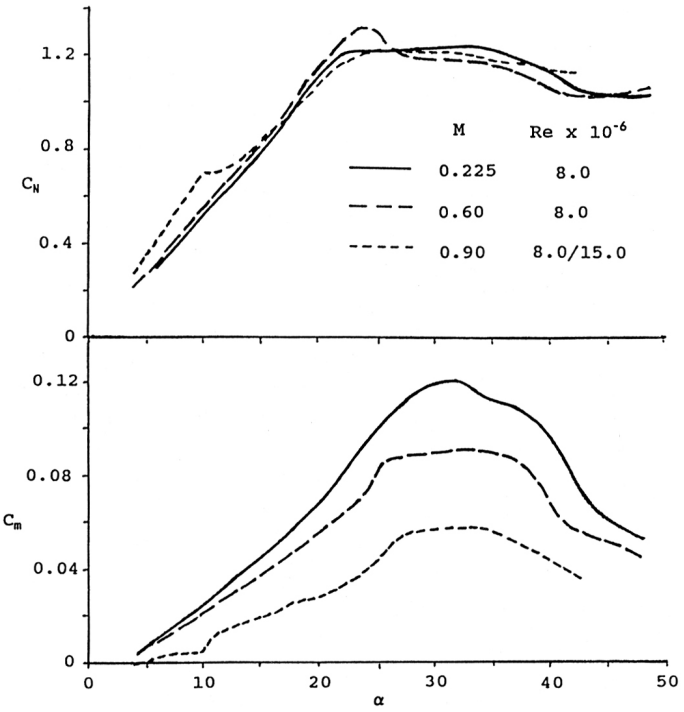

Figure 6: Effect of Mach Number on the Semi-Span Simple Straked Wing Model C_N and C_m in the NLR HST

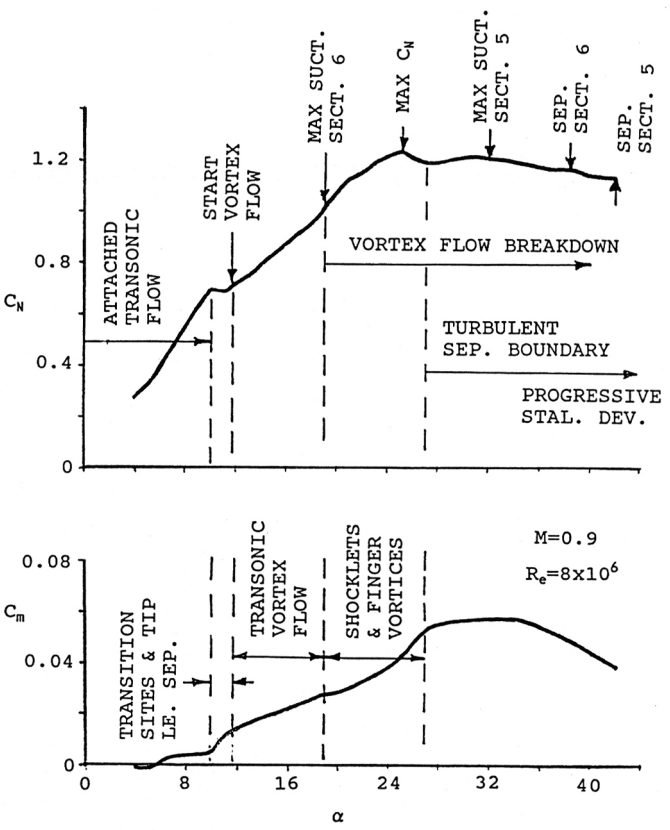

Figure 7: Steady Force and Moment Characteristics for the Simple Straked Wing Semi-Span Model at M = 0.9

Above 27.0 deg, the finger vortex/shocklet structure breaks down, and vortex burst continues to develop. In this region, leading edge separation is becoming dominant over the outer wing panel, as indicated in both the pressure data and appearance of a "turbulent separation boundary." At about 42 deg, the wing is fully stalled and the strake is stalling in a manner similar to that seen in the cases of lower speed flows.

4.0 STEADY AERODYNAMIC CHARACTERISTICS FOR M = 0.9

A comparison of the normal force and pitching moment curves for M = 0.225, 0.6, and 0.9 in Figure 6 shows that the characteristics at M = 0.9 are quite different, particularly at angles below about 12 deg. Figure 7 at M = 0.9 shows that the differences involve very complicated flow-field developments. The five flow regimes shown in Figure 7 will be discussed in following paragraphs. These are (1) attached transonic flow, (2) SITES and tip leading edge separation, (3) transonic vortex flow, (4) shocklets and finger vortices, and (5) turbulent separation boundary. The following discussions and data presentations present highlights of the complete discussions given in Reference 11 and the database given in Reference 12.

4.1 Attached Transonic Flow for M = 0.9

This is the simplest flow regime to discuss since it is restricted to the development of attached transonic flows with embedded multiple shocks and no significant separations. Two primary shocks are present: the forward shock that is swept, and the aft shock that is approximately parallel to the trailing edge. These characteristics are clearly seen in pressure data in Figure 8 at an angle of 8.39 deg. The forward shock sweep angle continually increases, and its point for crossing pressure Section 7 moves inboard from between pressure Sections 3 and 4 at 6.45 deg to between pressure Sections 1 and 2 at 9.38 deg. Trailing edge separation begins to appear in the tip pressures at Section 4 and 8.39 deg in Figure 8. The pressure data in Figure 8 at 10.39 deg represent the last data point prior to the onset of SITES at about 10.5 deg.

The high-speed CCD camera video frames in Figure 9 contain data for light sheet positions 8 and 9 corresponding to pressure Sections 6 and 7, respectively. The strake vortex is increasingly visible at position 9 as the angle is increased from 9.4 deg to 11.6 deg, at which point it is beginning to appear at position 8. Also at 9.4 deg, the "shear layer" that develops spanwise is seen as it wraps around the strake vortex. It is more visible at 11.6 deg in Figure 9 just after SITES onset.

This "shear layer" is the "gull-wing" pattern referred to in Reference 12 and is occasionally seen on aircraft flying at transonic speeds in humid air (for which many examples are given in Reference 15). Side view camera video frames in Figure 10 for angles increasing from 9.5 deg to 11.7 deg, respectively, provide streamwise cuts through the shear layer at sheet positions 1 and 14. A suggestion is posed that this shear layer represents the interface between (1) the outer flows that see the spanwise flow potential propagating from the inboard strake region, and (2) the inner supersonic flows near the wing surface. The justification for referring to this as a shear layer is the way that it wraps around the strake vortex in Figure 8, which also implies that its vorticity is the same sign as that of the strake vortex. Since the shear layer starts on the wing leading edge at the 76 deg/40 deg crank, further justification is given for this being a true shear layer whose vorticity is in the same direction as the strake vortex.

The side views also show the aft shock which, in agreement with pressure data, does not move significantly with increasing angle up to 10.31 deg. Pulsed laser recordings at sheet position 3 are shown in Figure 11 at 10.0 deg, where more detail is seen than in the side camera frames at position 1 in Figure 10. The shock is more clearly shown at 10.0 deg where a "lamda" shock with a thin boundary layer separation within the legs of the lamda is also seen. This condition at 10.0 deg is the precursor to SITES onset in Figure 11 at 10.5 deg.

Turning to sheet position 14 in Figure 10, development of the strake vortex is seen. This sheet position, as shown in Figure 2, is angled so that it always cuts through the strake vortex core no matter what the angle is. Vortex development is apparent at 9.5 deg in Figure 10 where the aft shock is also visible at about the same chordwise position as it is seen at sheet position 1 (in reference to the side wall "targets"). A core is also visible at 9.49 deg, and the aft shock is a little more defined. At 11.7 deg in Figure 10, both the vortex core and the aft shock are visible.

4.2 SITES and Tip Leading Edge Separation for M = 0.9

The pressure data shown in Figure 8 at 10.39 deg and 11.39 deg imply that a single, very catastrophic flow transition occurs between these two angles on the outboard wing. The same is true for the flow-visualization data in Figure 9 at 9.4 deg and 11.6 deg. This is not the case and, in actuality, two distinct flow transitions occur that are (1) SITES at just below 10.5 deg, and (2) wing tip leading edge separation at just below 11.0 deg.

The side view camera data in Figure 10 covers the angle range of 9.5 deg to 11.7 deg, which is similar to that in Figure 9 of 9.4 deg to 11.6 deg. The height of the shear layer at sheet position 1 increases at 11.75 deg in Figure 10. (Sheet position 3 shows the onset of SITES at 10.67 deg and wing tip leading edge separation at 10.86 deg in Reference 12.)

The weak side view camera images at position 3 in Reference 12 are augmented by the enhanced pulsed laser recordings at position 3 for the angles of 10.0, 10.5, and 11.0 deg in Figure 11. Multiple recordings were made at angles 10.5 deg and 11.0 deg to emphasize the unsteadiness of the flows at those angles. The data in Figure 11 at 10.0 deg show the development of the lamda shock structure and the thin shock-induced boundary layer separation within the lamda region. The data at 10.5 deg show the structure of SITES to extend much farther above the wing than had been previously thought. The heights of these excursions in the figure are on the order of 15% to 20% of the chord length. It is also of interest to note that the shock moves considerably forward with the onset of SITES at 10.5 deg as compared to 10.0 deg.

The character of wing tip leading edge separation at 11.0 deg just after transition is also shown in Figure 11. The turbulent shear layer is close to the wing and not much higher than the turbulent structures observed for SITES at 10.5 deg. The white regions above the turbulent shear layer indicate that this flow is still accelerated to supersonic speeds as was observed forward of the aft shock at 10.0 deg. The structure of the turbulent shear layer at 11.0 deg appears to be composed of small vortical structures and larger structures that have a wavelength of about 25% of the local wing chord.

Returning to the flow-visualization data in Figure 9 at 11.6 deg, it is easier to understand the flow structure indicated by the deterioration and distortion of the shear layer at sheet position 9. Also, it is now understandable why no indication of these transitions is seen at sheet position 8 in the same figure. The structure outboard of pressure Section 1 at sheet position 9 is extremely unsteady as can be seen in the high-speed video recordings. It is also the structure that will persist up to about 18 deg or 19 deg in the transonic vortex flow regime to be discussed below.

4.3 Transonic Vortex Flow for M = 0.9

In this flow regime, remnants of transonic flow with the forward shock present exist at pressure Section 1 at 12.39 deg and 13.41 deg as discussed in Reference 11. The forward shock moves inboard of this position at 14.42 deg. The peak in pressure in Section 6 near its intersection with pressure Section 1 starts increasing for angles higher than 14.42 deg as shown in Figure 8 at 16.43 deg. This peak continues to grow up to 18.45 deg, where it levels off at 19.45 deg and begins falling at 21.44 deg in Figure 8. A bump in the spanwise pressures in Section 7 centered on the intersection with pressure Section 1 is also seen to develop from 16.43 deg in Figure 8 to 21.44 deg.

This bump in Section 7 and the large peak in pressure Section 6 just discussed bear a strong resemblance to similar characteristics at M = 0.6 over the same incidence range as discussed in Reference 11. Since these characteristics at M = 0.6 were indicative of the wing vortex that starts at the leading edge crank, it is suspected that the same holds true for the M = 0.9 case. The transonic wing vortex is quite different from the conventional low-speed vortex and is suspected of being composed of shear layers to produce a more diffused vortical flow region.

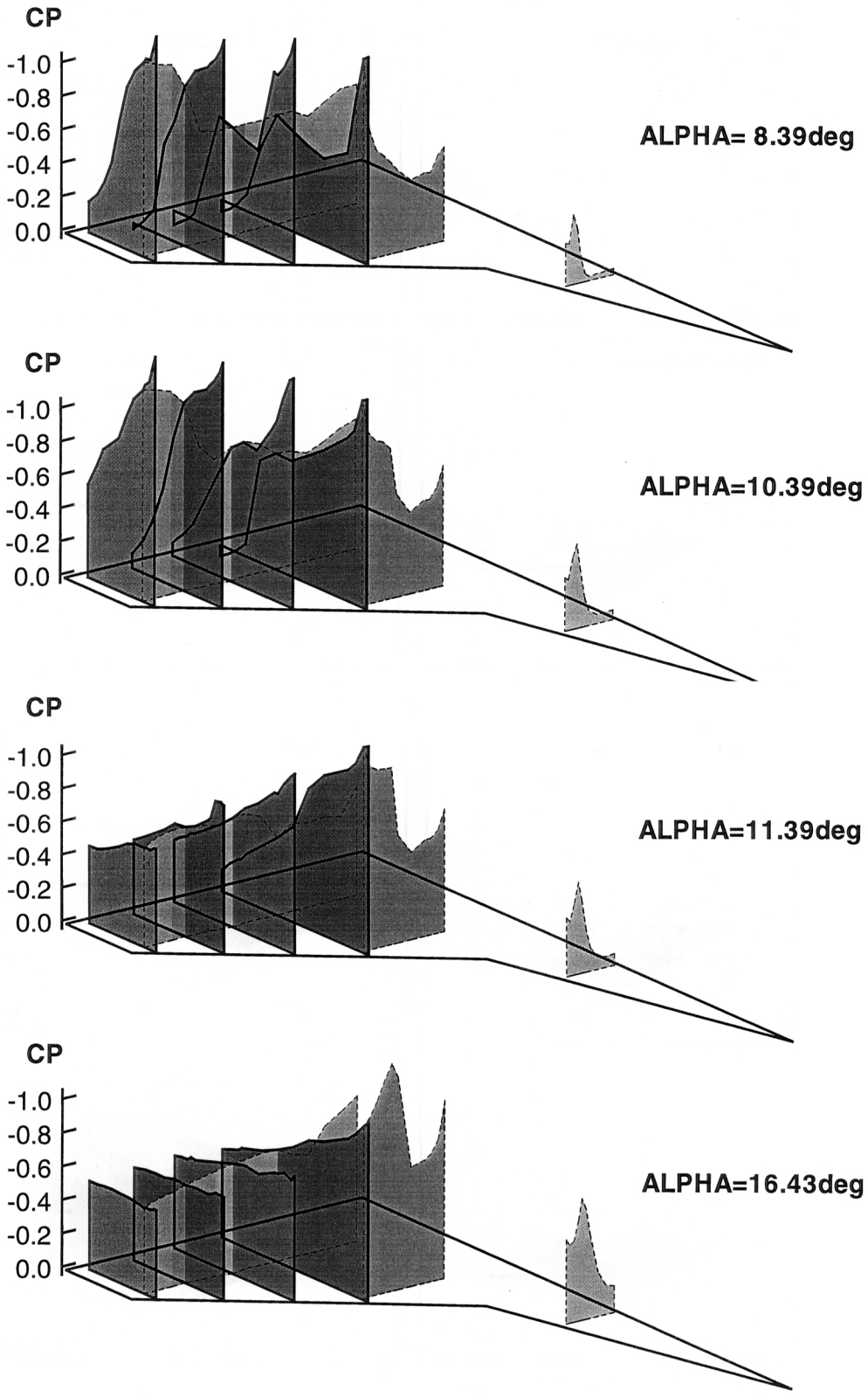

Figure 8: Steady Pressure Distributions, M = 0.9, Alphas = 8.39 deg – 36.39 deg

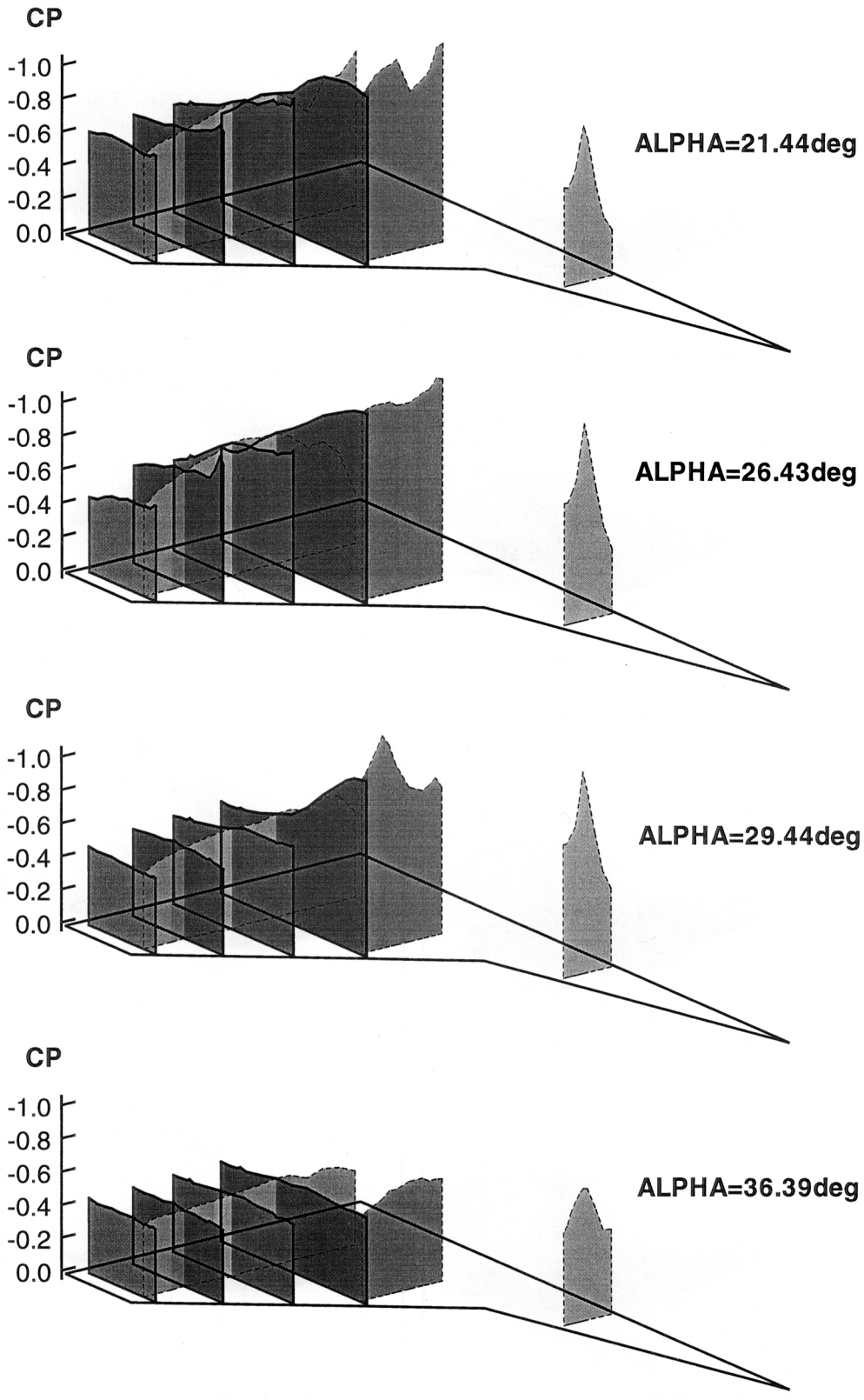

Figure 8: Concluded

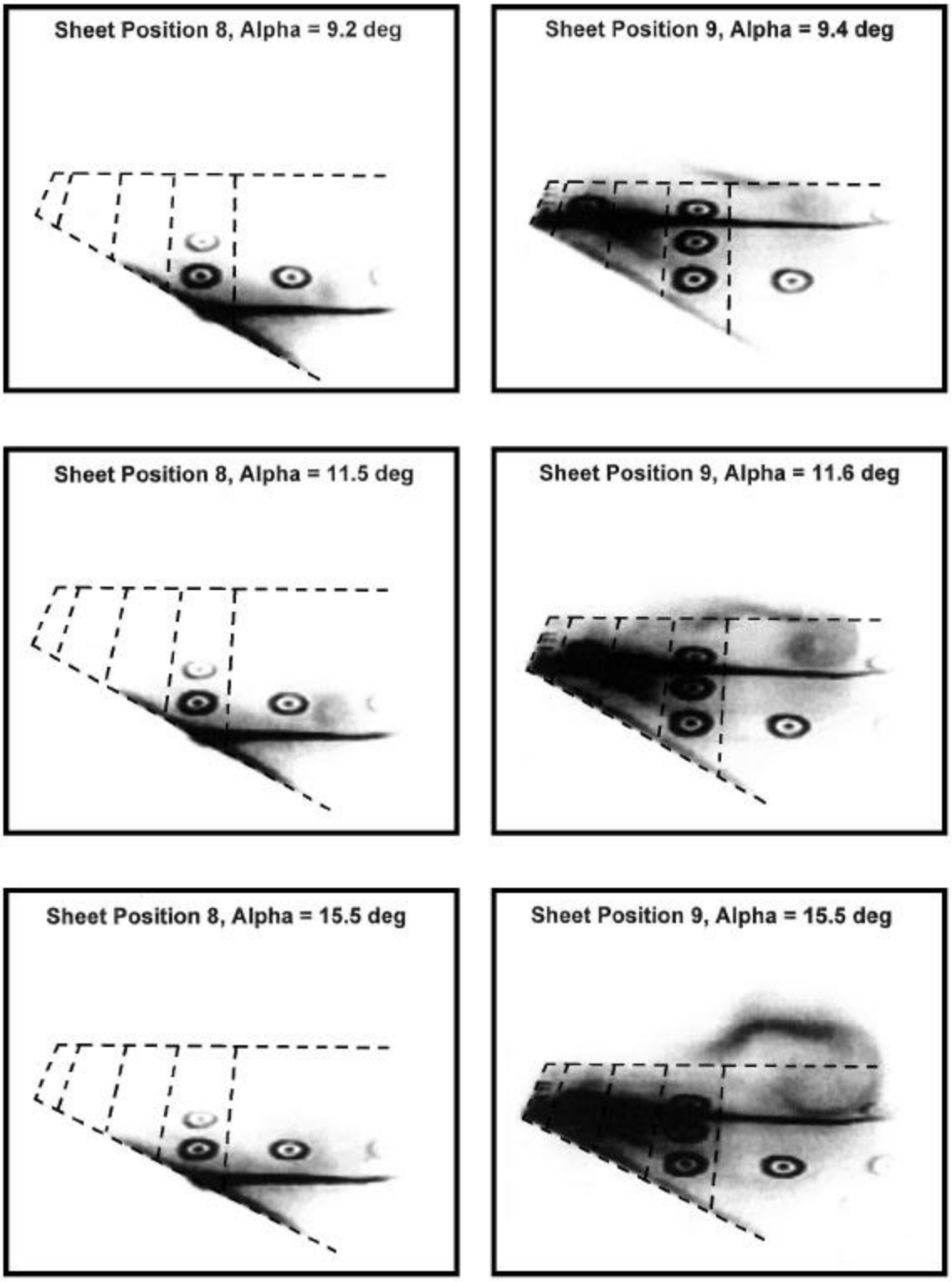

Figure 9: Steady Flow Visualization With the High-Speed CCD Camera, M = 0.9, Alpha = 9.4 deg – 29.2 deg

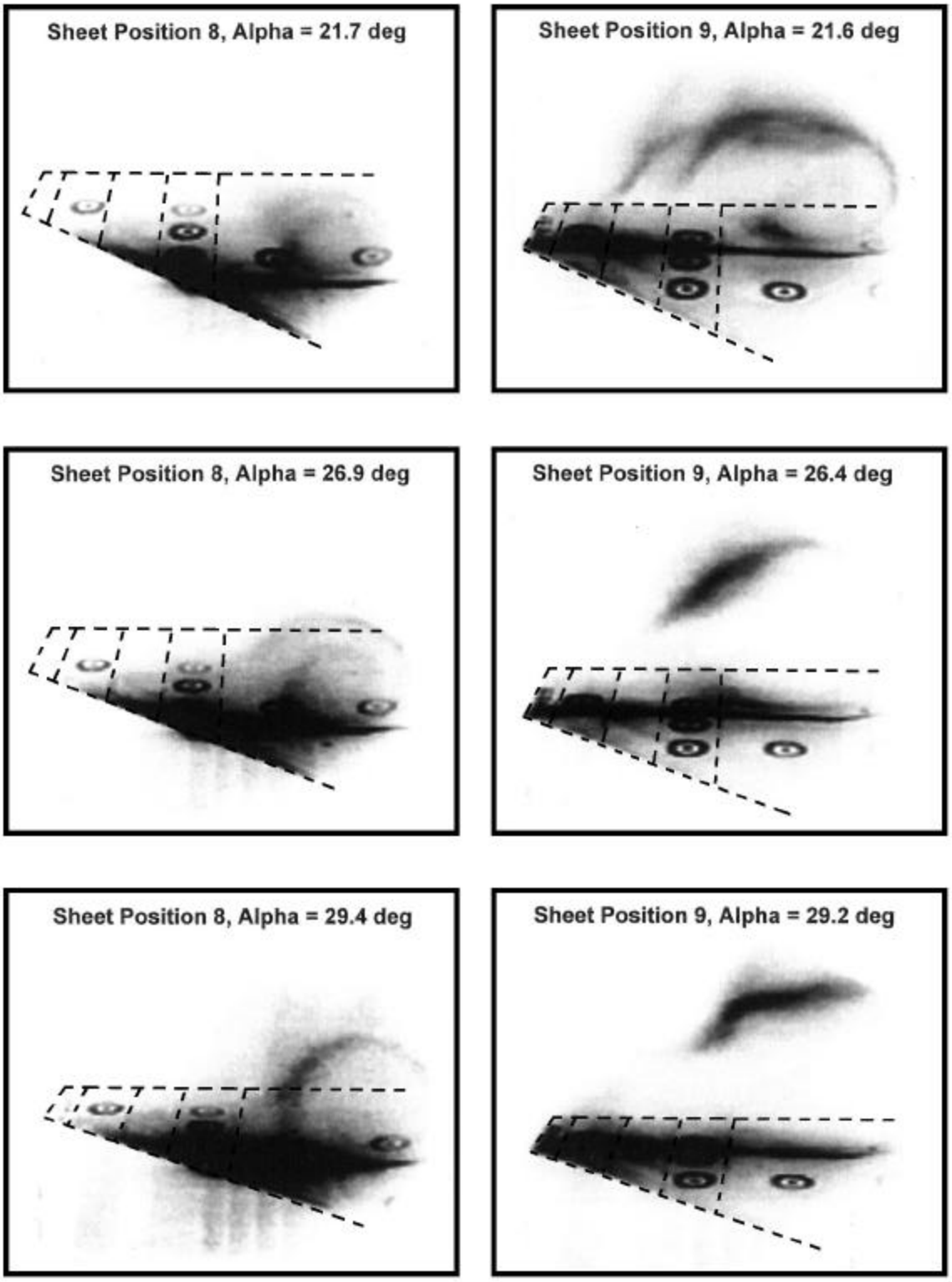

Figure 9: Concluded

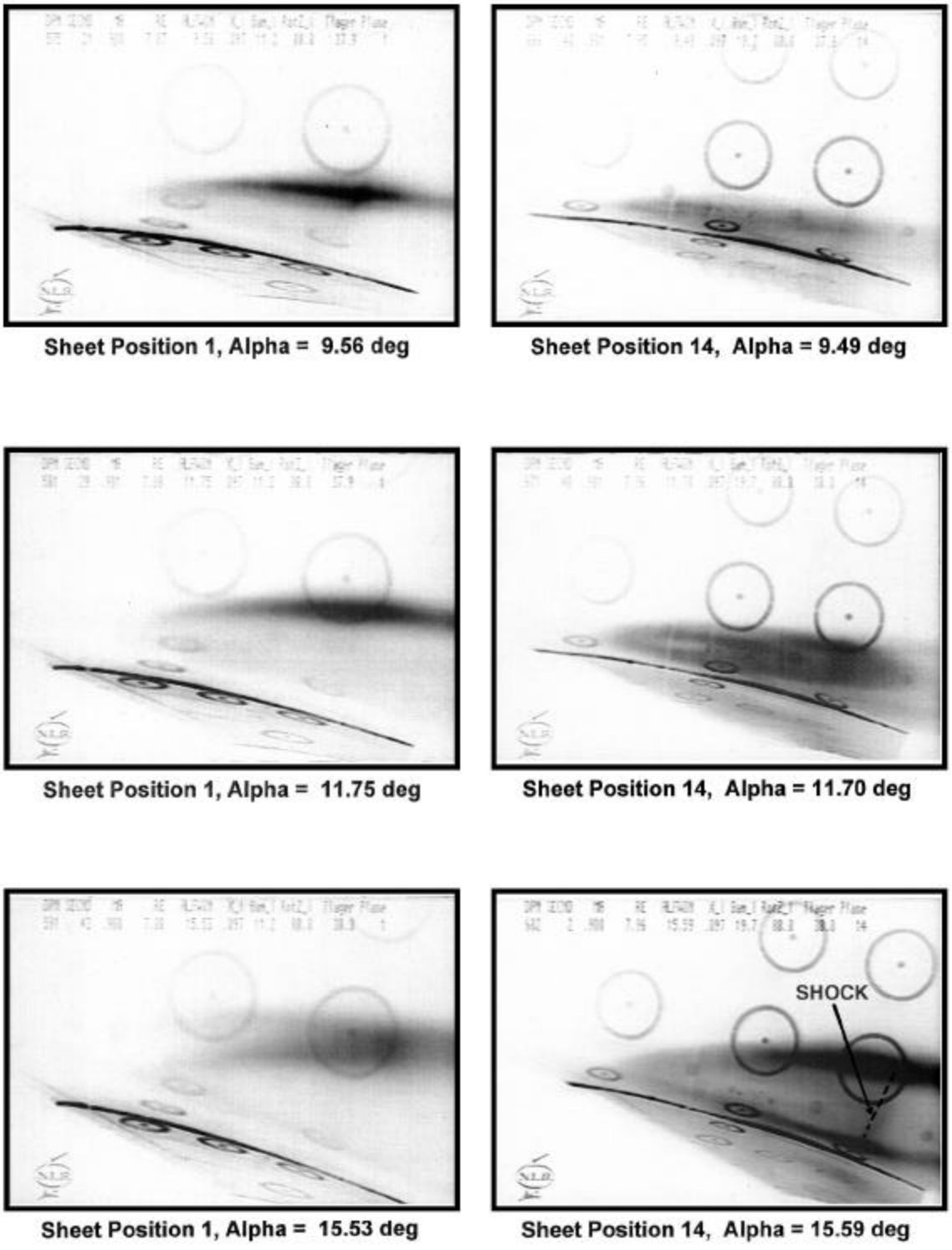

Figure 10: Steady Flow Visualization With the Normal-Speed Side View Camera, M = 0.9, Alpha = 9.5 deg – 29.5 deg

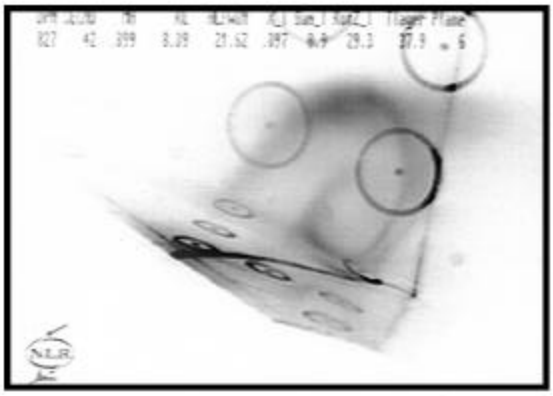

Sweeping Sheet, Alpha = 21.62 deg

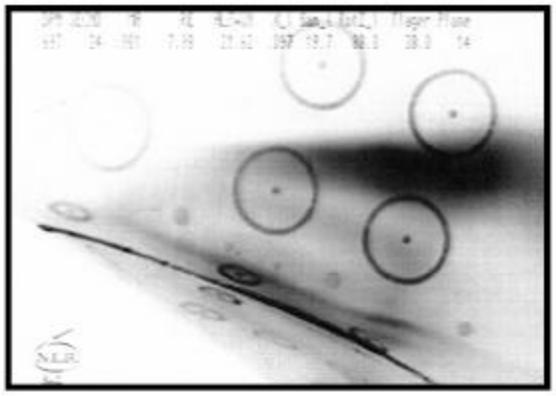

Sheet Position 14, Alpha = 21.62 deg

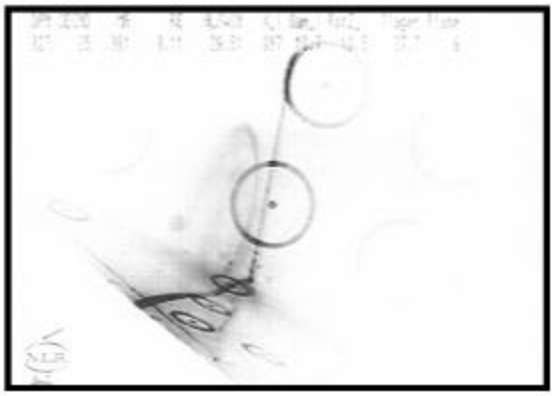

Sweeping Sheet, Alpha = 26.51 deg

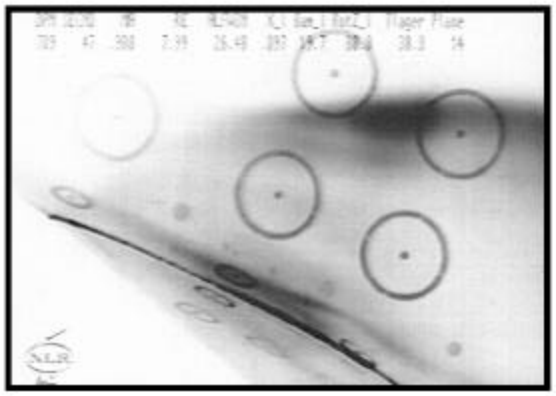

Sheet Position 14, Alpha = 26.48 deg

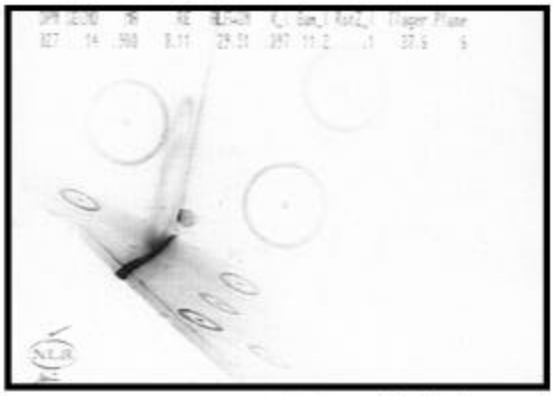

Sweeping Sheet, Alpha = 29.51 deg

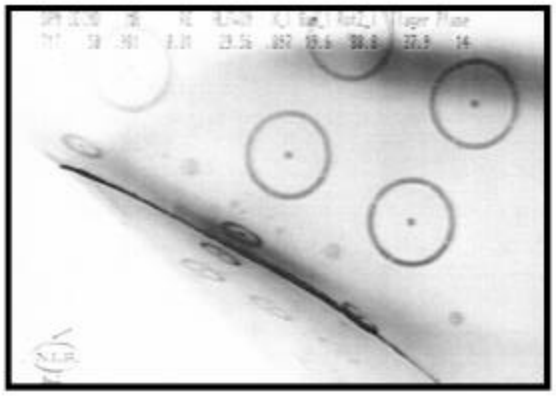

Sheet Position 14, Alpha = 29.56 deg

Figure 10: Concluded

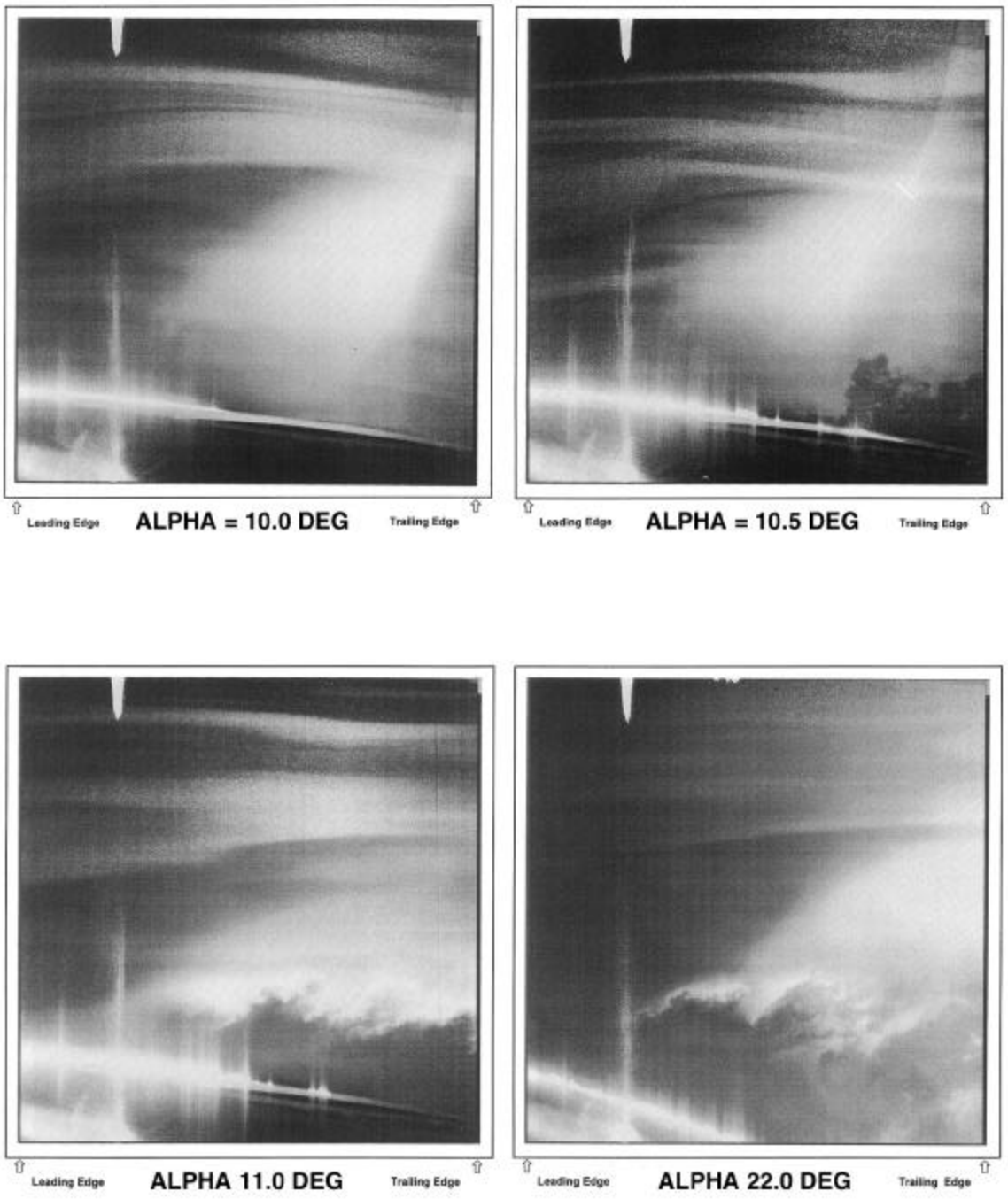

Figure 11: Pulsed Laser Reloading at Sheet Position 3 (80% Span) at M = 0.9, Alpha = 10.0 deg – 22.0 deg

Flow-visualization data corresponding to the pressure data discussed above are given in Figure 9, which shows a typical example at 15.5 deg. These data at sheet positions 8 and 9 show a fairly consistent development of a pattern that contains three basic elements: (1) the strake vortex (positions 8 and 9), (2) a strong shear layer that wraps around the strake vortex (position 9), and (3) outboard wing separation with an "s"-shaped transition in the shear layer at about pressure Section 1 (inboard chordwise row). The strake vortex image development is simply an extension of that seen at the lower angles, and the shear layer becomes stronger with increasing angle but does not change its character. Nothing is seen of the outboard separation development at 15.5 deg in Figure 9, but the s-transition at pressure Section 1 becomes more sharply defined at the higher angles up to 17.6 deg in Reference 12. The s-shape of this transition has all of the appearances of some type of vortical/shock interaction, but this has not been verified with data from this test.

The side view camera frame at sheet position 1 for the corresponding conditions discussed above is shown in Figure 10 for 15.5 deg. Shear-layer development at position 1 is seen as changing both in position (increasing height with increasing angle) and in character where it splits into two layers at 13.53 deg in Reference 12. The double shear layer shows that the lower layer appears to emanate from near the wing leading edge at sheet position 1. The upper layer also tends to line up with the upper boundary of the strake vortex image at sheet position 14 in Figure 10.

There is no difficulty in seeing the strake vortex developments at sheet position 14 in Figure 10. The core is clearly visible at 15.5 deg in Figure 10 where the aft shock appears within the vortex core and becomes another dominant feature in the images. Further developments up to 17.51 deg (Reference 12) show growth of the core and stronger interactions with the aft shock, both in the upper outer shear layer and the lower layer near the wing surface. The location of this shock at 15.5 deg is just aft of pressure Section 7 (and sheet position 9).

The leading edge separation outboard of the s-transition is very well identified with the pulsed laser recording frames at position 3 in Figures 11 at 11.0 deg. As discussed in Reference 11, the frames at 12.0 deg look similar to those at 11.0 deg but more developed and much more unsteady. This same structure is also seen at 18.0 deg, but a strong indication that a transition is about to take place is shown in Reference 11. Discussions are also presented in Reference 11 that describe this structure as being vortical in nature with wave lengths on the order of 15% to 20% of the local chord.

4.4 Shocklets and Finger-Vortex Structure for M = 0.9

In Reference 11, the process is described in which at angles above 18.45 deg, the pressure data show a continuous deterioration of the wing vortex signature at pressure Section 6. The growth of the corresponding pressure peak at this section for angles up to 18.45 deg stops at 19.45 deg. This growth is reversed until the peak disappears by about 25.43 deg. Wing pressures overall, however, experience a slow, steady growth with exception of the wing vortex region. Typical pressure distributions in this flow regime are shown in Figure 8 at 21.44 deg and 26.43 deg. The strake vortex also grows in strength, as indicated by the pressures at Section 5 in Figure 8. These observations are in agreement with the normal force and moment trends seen in Figure 7 where peak normal force occurs at about 25 deg, and pitching moment is increasingly more nose-up until 27 deg to 28 deg, where it levels off.

The corresponding flow-visualization data are shown in Figure 9 for sheet positions 8 and 9. A typical view for this flow is seen in Figure 9 at 21.6 deg where multiples of the s-transition structure appear at sheet position 9 in the region outboard of pressure Section 1 as the shear layer alters its shape dramatically. The strake vortex signature does not change much until about 23.4 deg, where it begins to widen significantly to the condition shown at 26.4 deg in Figure 9.

The most notable features in this flow regime are the multiple s-transitions with extensions into the upper flows that appear to be shocks. It was postulated that these flow features were composed of multiple vortical structures emanating from the leading edge, which led to the term "finger vortices." Each set of those finger vortices had an apparent shock associated with it, which likewise led to the term "shocklets." The best view of

the shocklet and finger-vortex structures is shown in Figure 9 at 21.6 deg. In this example, two sets are seen where the inboard set corresponds approximately to pressures Section 2 and the outboard set to Section 3.

Another interesting observation in Figure 9 at 21.6 deg and 26.4 deg is the development of the strake vortex image at sheet position 8. This observation centers on the abrupt termination of the shear layer wrapping around the strake vortex. Following the layer from the vortex core in a counterclockwise direction in Figure 9 at 21.6 deg, the layer stops outboard and above the core with a shape that looks similar to the s-transition discussed earlier at sheet position 9 (at 15.5 deg). Although the image is not as strong at sheet position 8, it is repeatable and appears at the angles consistent with breakdown of the wing vortex seen in the pressure data over the incidence range of 19.45 deg through about 24.45 or 25.43 deg. This observation lends more credibility to the postulation presented in Reference 11 that the forward shock and the wing vortex are combined into a single-flow phenomenon.

The side view camera frames shown in Reference 12 for this flow regime are also very interesting and provide streamwise cuts through the structures discussed based on the spanwise sheet positions. Sheet position 4 at the wing tip shows a definite development of a vortex-looking streak that emanates from the wing leading edge. As wing incidence increases, this flow feature also shows a corresponding increasing angle of separation above the wing. Sheet position 1 shows that the double shear layer structure at 18.50 deg changes to a more diffuse structure and increasing height above the wing as the angle is increased up to 25.57 deg. Another new structure shown at sheet position 1 near the wing surface moves forward from the trailing edge of the wing starting at 21.67 deg. It also appears at sheet position 3 at 25.67 deg. Motion of this structure as seen in the videotapes is very unsteady and appears to be associated with breakdown in the strake vortex.

Sheet position 14 shows the strake vortex development up to 26.5 deg in Figure 10, where progression of vortex growth and shock development in the range of 21.6 deg to 26.5 deg are consistent and steady with no apparent strong transitions. The shock-induced separation of a layer near the wing that was discussed previously in Section 4.3 does not move until the angle reaches 23.55 deg where it starts moving forward. At 26.5 deg in Figure 10, it has moved forward enough to be in view of spanwise sheet position 9. Referring to Figure 9 at 21.6 deg and 26.5 deg, a distinct change is seen in the portion of the shear layer that is below the strake vortex near the wing. It is also shown by the pressure data in Figure 8 at 26.43 that a significant drop occurs in the pressures at Section 7 corresponding to the strake vortex location. Thus, it appears that the maximum normal force seen in Figure 7 occurs at about the time this shock-induced separation begins to move rapidly forward.

The sweeping sheet frames also shown in Figure 10 for 21.6 deg, 26.5 deg, and 29.5 deg provide data that tie together the characteristics discussed above for sheet positions 1, 3, 8, 9, and 14. This sweep shows that the finger-vortex/shocklet/shear-layer structure is continuous from the wing leading edge. It also shows that the strake vortex is the primary flow feature over this angle range, and that it is well formed over the wing.

The pulsed laser recording at sheet position 3 and 22.0 deg is included in Figure 11, which shows a very “stable” separated flow that does appear to be composed of multiple “finger vortices,” above which is a supersonic region that must terminate in a shock at some point. Since sheet position 3 is close to the outer finger-vortex/shocklet structure seen in Figure 9 at 21.6 deg, Figure 11 at 22.0 deg does apparently provide a detailed view of that phenomenon and verify both its character and relative stability as was noted earlier.

4.5 Turbulent Separation Boundary for M = 0.9

Above angles of 25.43 deg, the pressure data show that the wing tip is stalled and remains so, as evidenced by the pressures at row 4 in Figure 8 at 26.43 deg and 29.44 deg. A continuous breaking down of pressures at the inboard rows 2 and 3 at these two angles is indicative of progressive stalling of the outboard wing panel. Accompanying this breakdown is a rising peak in the pressure row 6 distribution, which corresponds to a “new” wing vortex. The crossing of this wing vortex at the forward part of pressure row 1 is also seen at 29.44 deg in Figure 8 where, by the angle of 32.40 deg, this growth process has broken down (Reference 12). By 36.39 deg in Figure 8, the wing aft of the leading edge crank is almost fully stalled. The strake vortex pressure

peak continues to grow until it reaches a maximum at 30.46 deg and 32.40 deg, after which it deteriorates at 34.42 deg and further at 36.39 deg as shown in Figure 8.

The flow-visualization data in Figure 9 at 26.4 deg and 29.2 deg for sheet positions 8 and 9 show a continuous breakdown of the strake vortex at position 9. At 29.4 deg in Figure 9, the strake vortex breakdown reaches sheet position 8, and the image at sheet position 9 takes on a new character, which is seen to evolve at the angles of 26.4 deg and 29.2 deg. As shown in Reference 12, this structure remains dominant until 34.0 deg at sheet position 9 where it becomes less distinct and picks up a weak outboard extension that is also seen at 36.0 deg. The image at sheet position 8 shows a continuous change up to 34.0 deg where at 36.0 deg it becomes very diffused (Reference 12) as is consistent with the weak vortex signature in the pressures at row 6 for 36.39 deg in Figure 8.

Images at sheet position 9 in Figure 9 at 26.4 deg and 29.2 deg are indicative of very turbulent, full-span leading edge separation, which is bounded by a likewise very turbulent shear layer. This observation was the basis in Reference 9 for referring to this flow regime as “turbulent separation boundary.” The shape of this boundary is defined by the wing tip and leading edge up to the strake wing crank where transition into the strake vortex structure occurs. This intersection of two different flow fields is probably the source of the kink seen in the sheet position 9 image in Figure 9 at 29.2 deg. There is a strong similarity between this kink and the “s-transition” structure discussed earlier for transonic vortex flow at 15.5 deg in Figure 9.

Side view images in Reference 12 at sheet position 14 show that the strake vortex structure changes at 27.61 deg and remains the same to the highest angle of 34.61 deg for which the image at 29.56 deg in Figure 10 is typical. This structure is the single outer shear layer wrapping around the burst strake vortex, as shown in Figure 9 at 29.2 deg.

Returning to the “new” wing vortex observed in the pressure data between 26.43 deg and 34.42 deg, the flow-visualization structure that is associated with its position appears to be the outboard end of the strake vortex shear layer next to the wing. This is seen as a bump in Figure 9 at sheet position 9 and 26.4 deg near pressure row 1, which has almost disappeared at 27.7 deg. A similar structure is seen in the same figure at about mid-span of sheet position 8 where the outer shear layer next to the strake vortex is leaving the wing surface. Additional data are shown in Reference 12, where these structures at positions 1, 3, 8, and 9 all line up with the leading edge crank at 26.4 deg as well as other angles. It is suspected that the associated common-flow phenomenon is an extension of the reverse-circulation secondary vortex that exists on the strake as it passes over the wing.

5.0 UNSTEADY AERODYNAMIC CHARACTERISTICS FOR M = 0.9

This section addresses the effects of model pitching motion on the flow fields discussed above in Section 4.0. Emphasis will be placed on the differences observed between pitching-up and pitching-down motions, as well as how they relate to conditions for the stationary model at similar angles. The five flow regimes to be discussed will be: (1) attached transonic flow, (2) SITES and tip leading edge separation, (3) transonic vortex flow, (4) shocklets and finger vortices, and (5) turbulent separation boundary. The effects of pitch-up and pitch-down during the cycle will be emphasized for each of the five flow regimes.

The variation of wing normal force, C_N , and pitching moment, C_m , is shown in Figure 12 at M = 0.9 for the model at static conditions and pitch-up, pitch-down for a (1-cos) motion at 3.8 Hz. With this type of motion, the wing starts from rest at 7.2 deg, reaches maximum incidence of 37.7 deg, and returns to rest at 7.2 deg where the motion is described by a (1-cos ωt) wave form. The dynamic effects seen in Figure 12 at M = 0.9, compared to those in Reference 11 at M = 0.6, are much less pronounced because with a constant frequency of 3.8 Hz but a higher velocity, the non-dimensional pitch rate is proportionately smaller by the ratio of 0.6/0.9, as discussed in Reference 8.

Dynamic-pressure data are shown in Figure 13 for pitch-up and in Figure 14 for pitch-down. Flow-visualization data are shown in Figure 15 for pitch-up and Figure 16 for pitch-down. The following discussions will address these data first for pitch-up and second for pitch-down.

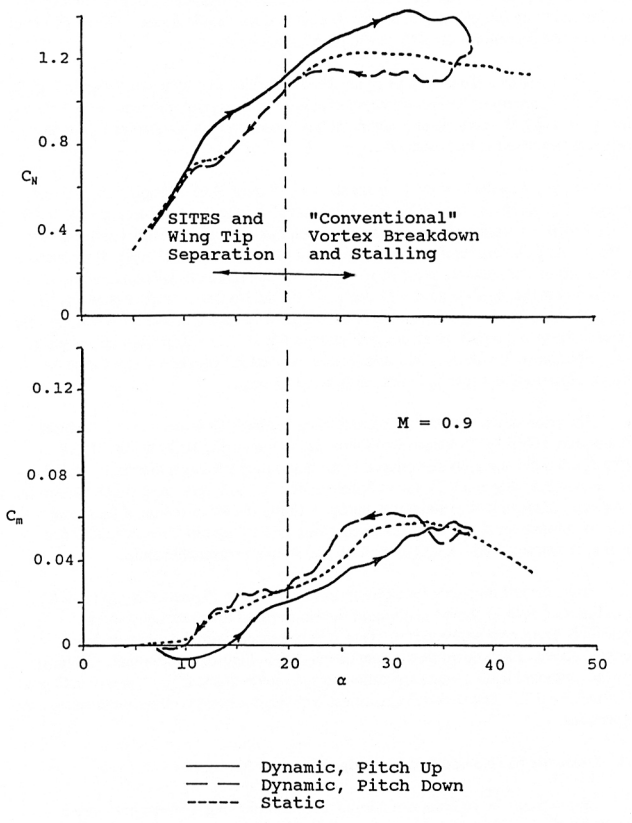

Figure 12: Pitch-Up/Push-Over Maneuver Motion Between Alpha = 7 deg and Alpha = 37 deg for M = 0.90

5.1 Effects of Pitch-Up

The pressure data for pitch-up are shown in Figure 13 for angles that correspond to those for steady flow in Figure 8. Pressures at 8.60 deg in Figure 13 are similar to those in Figure 8, but tend to show a more aft loading on the outboard pressure rows. The same is true at 10.73 deg in Figure 13, compared with 10.39 deg in Figure 8, which indicates that SITES is not fully developed in the dynamic case in Figure 13. At 11.62 deg in Figure 13, the pressures are similar in trend to those at 10.73 deg and 8.60 deg in the same figure, but are quite different from those in Figure 8 at 11.39 deg, which is the condition for leading edge separation. The differences between unsteady (Figure 13) and steady (Figure 8) pressures are: (1) more aft loading for unsteady flow that corresponds to a more nose-down pitching moment, and (2) overshoot of attached flow characteristics.

Flow-visualization data in Figure 15 for pitch-up show a continuous development of the shear layer and an increasingly prominent strake vortex for the angles of 9.26 deg and 11.96 deg. This is in agreement with the pressure data at similar angles in Figure 13. Comparing 11.96 deg in Figure 15 with 11.6 deg in Figure 9 for steady flow, the leading edge separation that occurs at about 11.0 deg in steady flow has not occurred at 11.96 deg for unsteady flow.

On pitch-up, variations of normal force and pitching moment in Figure 12 indicate that the transition to SITES and leading edge separation is more diffuse and begins at about 12 deg to 13 deg. The pressure data in Reference 13 for pitch-up show that SITES probably did not occur, but the transition to leading edge separation had occurred by 13.87 deg. The dynamic effects in the pressure data for this transition are more confined to the wing tip section. The dynamic effects in the flow-visualization data for pitch-up in Figure 15 show that at 15.87 deg, the leading edge flow separation is more outboard and less pronounced than is shown for steady flow at 15.5 deg in Figure 9. This is in agreement with the pressure data trends in comparing Figure 13 at 17.85 deg and Figure 8 at 16.43 deg.

Normal force variations on pitch-up in the vortex flow regime, to about 20 deg in Figure 12, have a higher level than those for static data. Pitching moment is less nose-up than static data, indicating that the additional lift is aft. The unsteady pressure data typical of vortex flow in Figure 13 at 17.85 deg show a much stronger strake and wing vortex lift than that for steady flow at 16.43 deg in Figure 8. Flow-visualization data in Figure 15 at 15.87 deg show a more tightly wound unsteady strake vortex, compared with the steady strake vortex in Figure 9 at 15.5 deg. In Reference 13, the unsteady flow-visualization data during pitch-up show that the unsteady images at a given angle in the vortex flow regime correspond to steady images at about a 1.0 to 1.5 deg lower angle. This is typical of aerodynamic lag in vortex flows where, at transonic speeds, the angle for transition to the shocklet/finger-vortex structure is delayed from the steady value of about 18.5 deg to the unsteady value of 19.5 deg.

The pitch-up trend in the shocklet/finger-vortex regime, for normal force above 20 deg shown in Figure 12, continues that trend begun in the vortex flow phase just discussed. The maximum normal force is achieved at about 32 deg. Pitching moment also continues the trend of being less nose-up than the static data, but is

running about parallel to that curve. Unsteady pressure data corresponding to this flow regime are shown in Figure 13 at the angles of 20.85 deg, 26.92 deg, and 29.71 deg. The equivalent steady data are shown in Figure 8 at the angles of 21.44 deg and 26.43 deg. As discussed in Reference 11, the trends in pressure distributions are different where the unsteady lift distribution is more inboard and the maximum angle range for unsteady flow has been extended by about 4 deg to at least 29.71 deg. Flow-visualization data for pitch-up are shown in Figure 15 at the angles of 21.99 deg, 26.96 deg, and 29.20 deg, which correspond to their steady counterparts in Figure 9 at 21.6 deg and 26.4 deg. Similarities between the two data sets at the two lower angles track similarities and differences in the pressure data. At 29.20 deg in Figure 15, the flow visualization is very similar to that at 26.96 deg in Figure 15, but much different from that at 29.2 deg in Figure 9 for steady flow. Thus, the dynamic effects on pitch-up in the shocklet/finger-vortex regime are even more pronounced than at the lower angle flow regimes.

The pitch-up curve in Figure 12 for normal force shows that the maximum value is achieved at about 32 deg, which corresponds to the dynamic transition from shocklet/finger-vortex flow to the turbulent separation boundary flow. After this point, the normal force quickly falls off, and pitching moment trends for pitch-up approach and follow the steady trend. Unsteady pressure data at 35.77 deg in Figure 13 are more similar in distribution to the steady data in Figure 8 at 29.44 deg than the steady pressures at 36.39 deg. In this comparison, the dynamic displacement in equivalent angle for turbulent separation boundary flow is about 6 deg as compared with 4 deg noted above for the shocklet/finger-vortex flow regime.

5.2 Effects of Pitch-Down

In the following discussions for pitch-down, the order will be reversed to decreasing angle to follow increasing time. This approach permits a logical treatment of the lagging characteristics typical of high-incidence unsteady flows and is the reason for reverse ordering of the pressure and flow-visualization data in Figures 14 and 16.

The pitch-down curves after peak incidence of 37 deg in Figure 12 for normal force show that the fall-off from the maximum value for pitch-up is very rapid. Pitching moment is momentarily more nose-down, but quickly becomes more nose-up than the steady data below about 32 deg. The unsteady pressure data for pitch-down in the turbulent separation boundary flow regime are shown in Figure 14 at the angles of 36.09 deg, 29.88 deg, and 27.04 deg. The corresponding steady data are shown in Figure 8 at 36.39 deg and 29.44 deg. The highest angle unsteady and steady data are very similar and are indicative of almost fully stalled flow with some residual vortex lift that exists at pressure Section 5 on the strake. In comparison with steady data in Figure 8, the persistence of outer wing separated flow continues dynamically down to 27.04 deg in Figure 14, but strake vortex flow is developing much more rapidly inboard. These mixed flow trends are also typical of low-speed conditions and explain why the pitch-down normal force trend is very near that of steady flow, and that pitching moment is more nose-up. Because of the high angles, however, the flow-visualization data for unsteady flow in Figure 16 at 29.96 deg and 25.76 deg are not much different than those for steady flow at 29.2 deg and 26.4 deg in Figure 9.

During pitch-down, the normal force and pitching moment data in Figure 12 show that the transition from turbulent separated boundary flow regime to shocklet/finger-vortex flow occurs at about 24 deg or at about 2 - 3 deg lower than for steady flow. This is more noticeable in the pitching moment for reasons discussed above. Pressure data for pitch-down in Figure 14 at 20.77 deg are similar to those for steady flow in Figure 8 at 21.44 deg. A similar comparison is seen for the unsteady flow-visualization data in Figure 16 at 21.99 deg and steady data in Figure 9 at 21.6 deg. These comparisons are in agreement with the similarities seen between steady and unsteady pitch-down normal force and pitching moment trends in the 18 deg to 22 deg range in Figure 12.

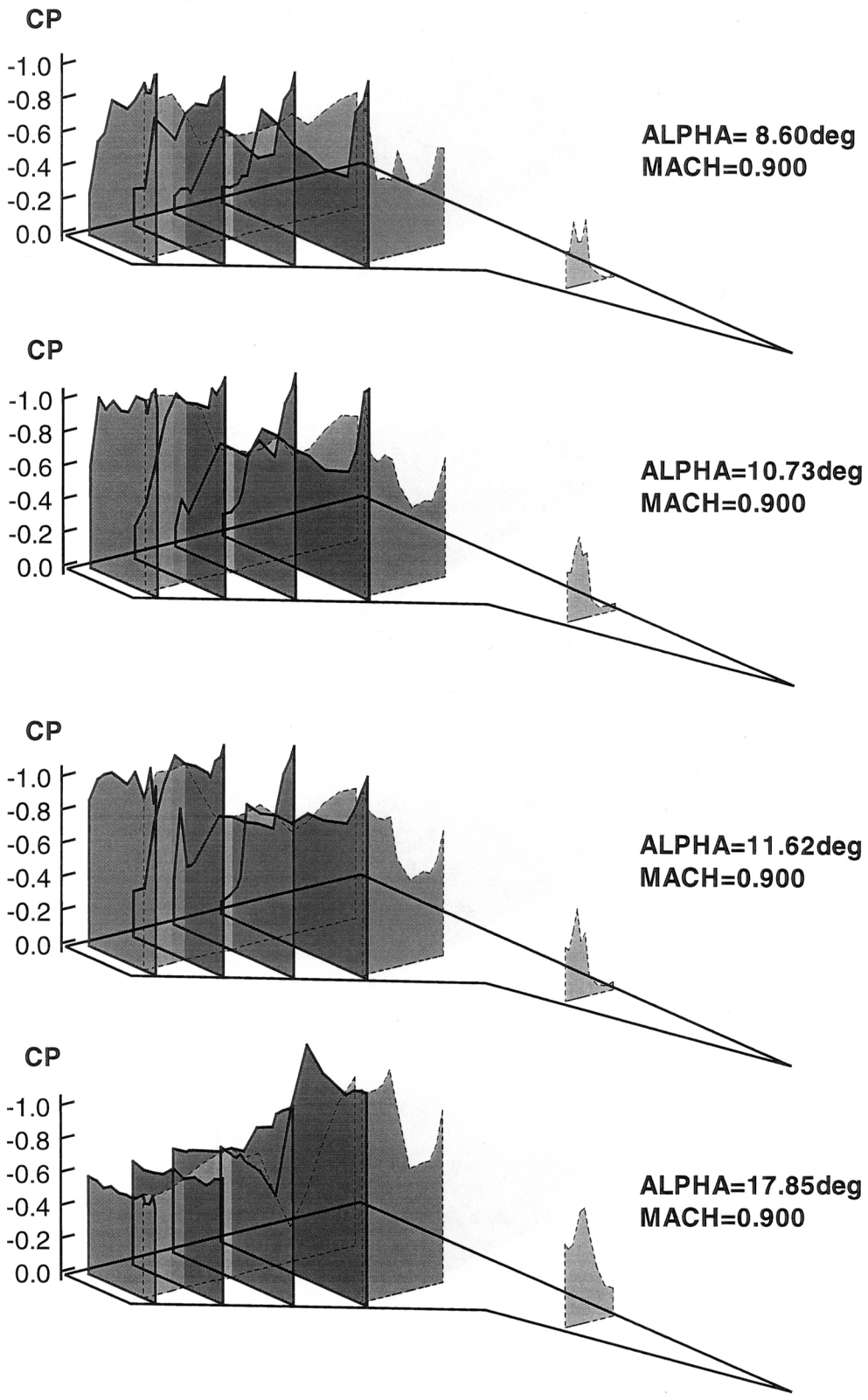

Figure 13: Selected Unsteady Pressure Distributions, M = 0.9, for Pitch-Up From 7.2 deg – 37.7 deg at 3.8 Hz

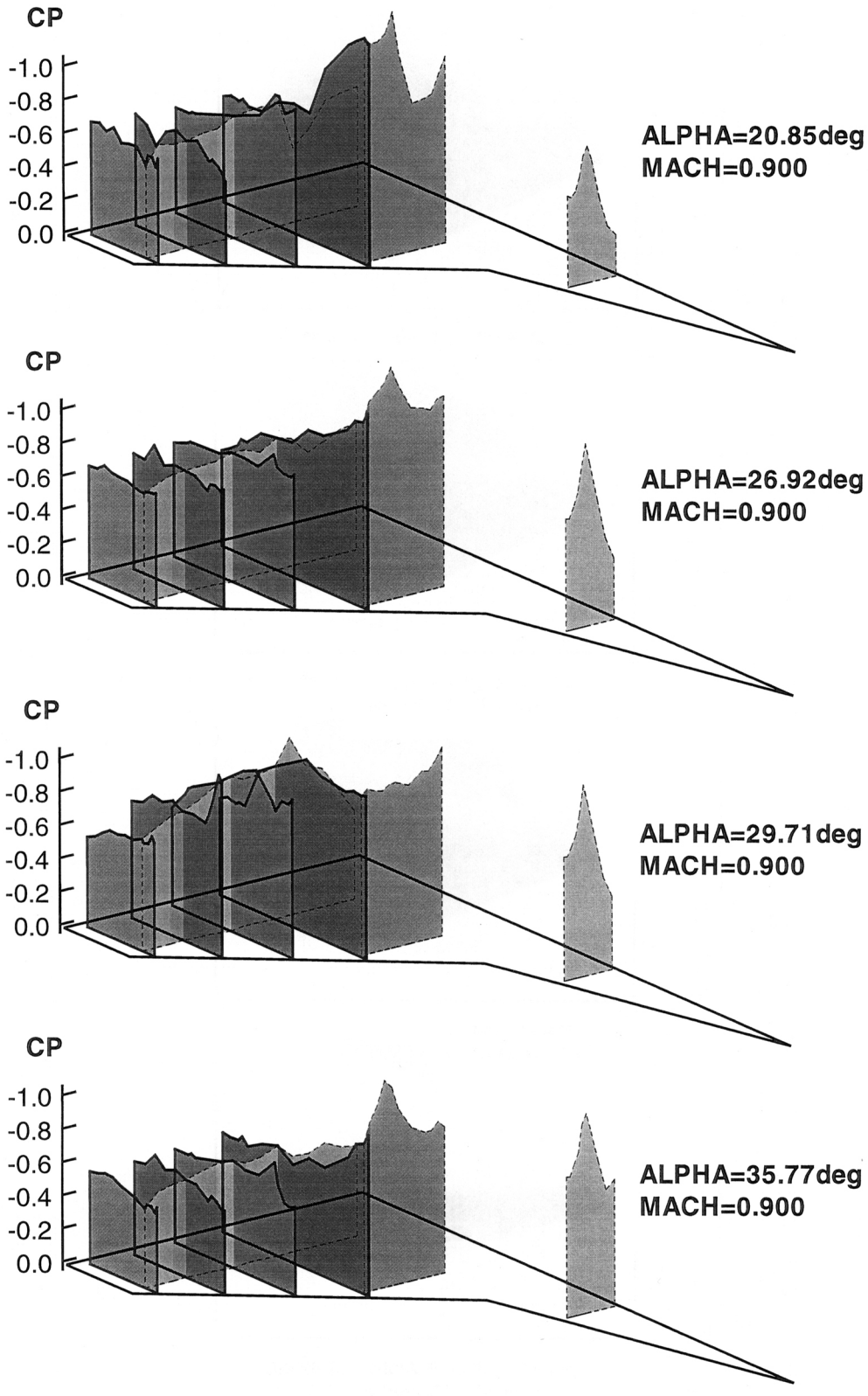

Figure 13: Concluded

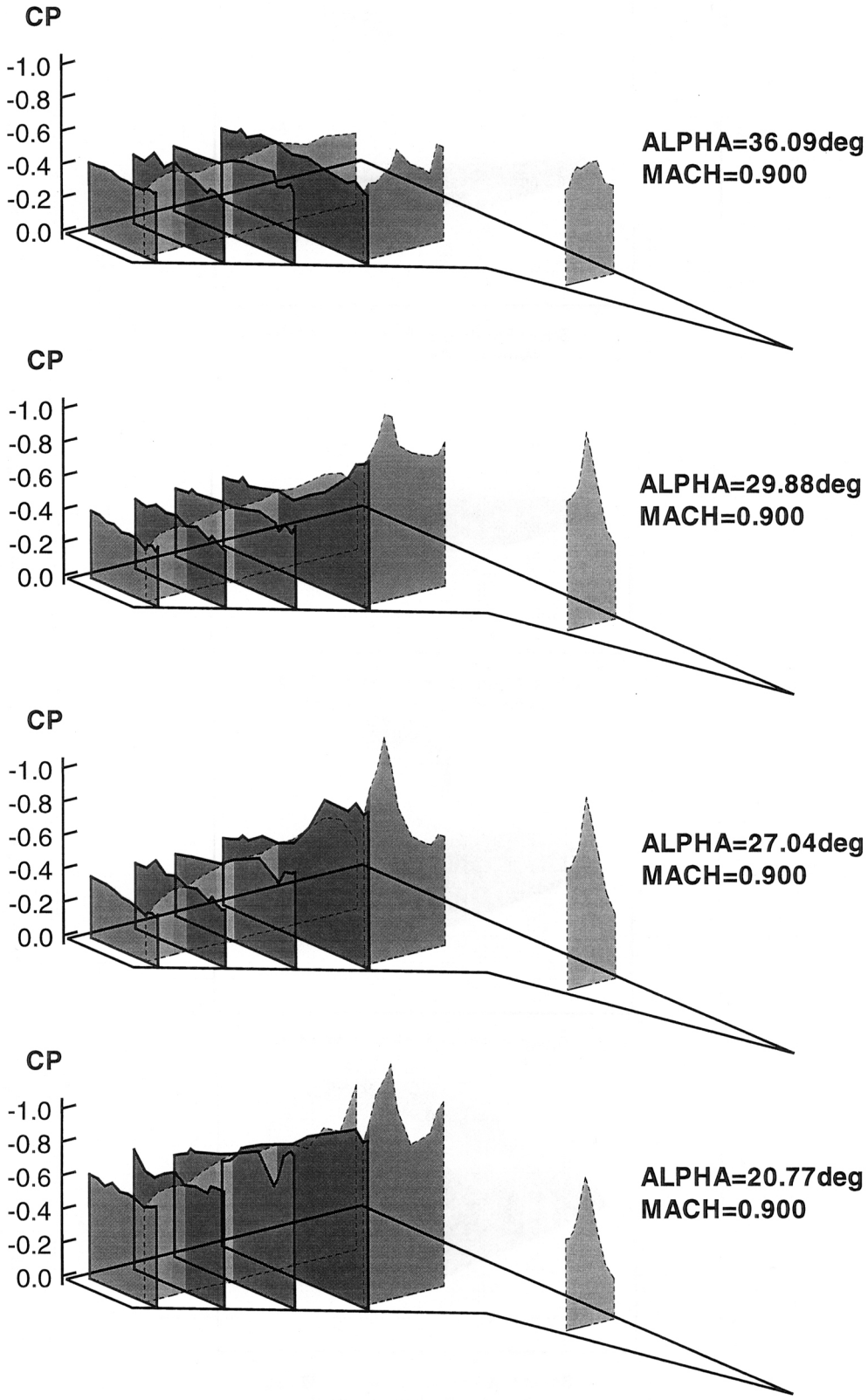

Figure 14: Selected Unsteady Pressure Distributions, M = 0.9, for Pitch-Down From 37.7 deg – 7.2 deg at 3.8 Hz

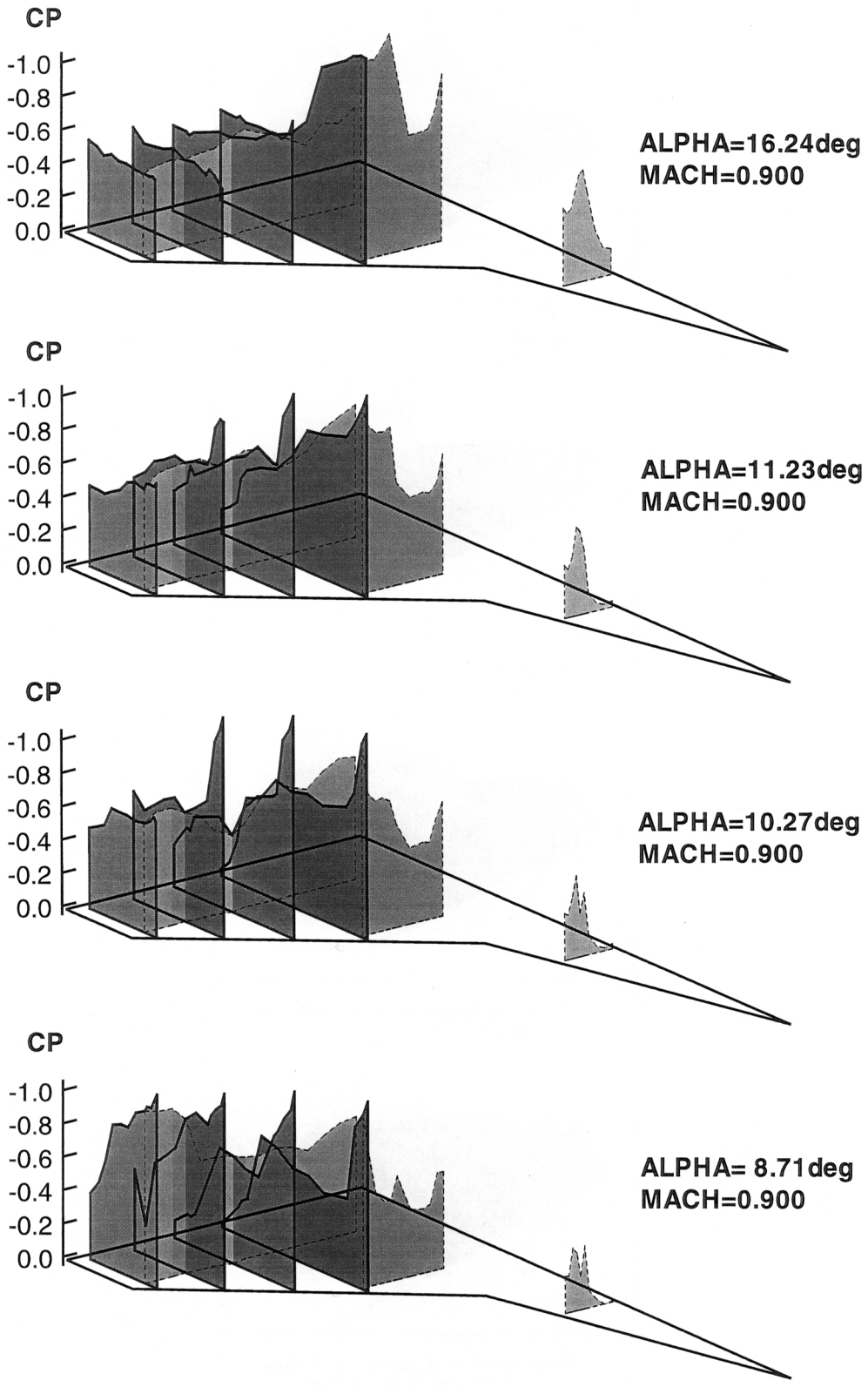

Figure 14: Concluded

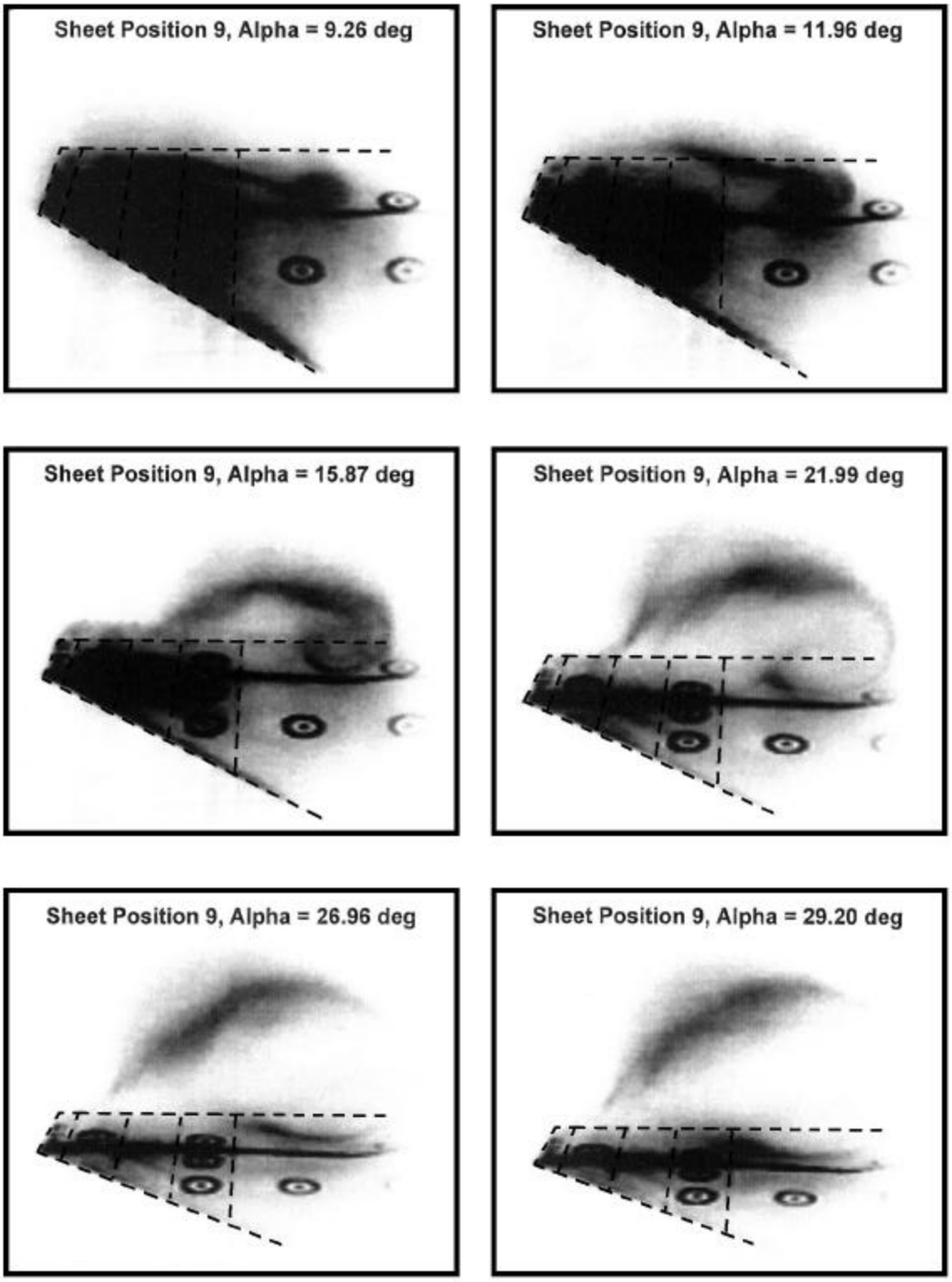

Figure 15: Unsteady Flow Visualization With the High-Speed CCD Camera, M = 0.9, Alpha = 9.01 deg – 34.97 deg, Pitch-Up

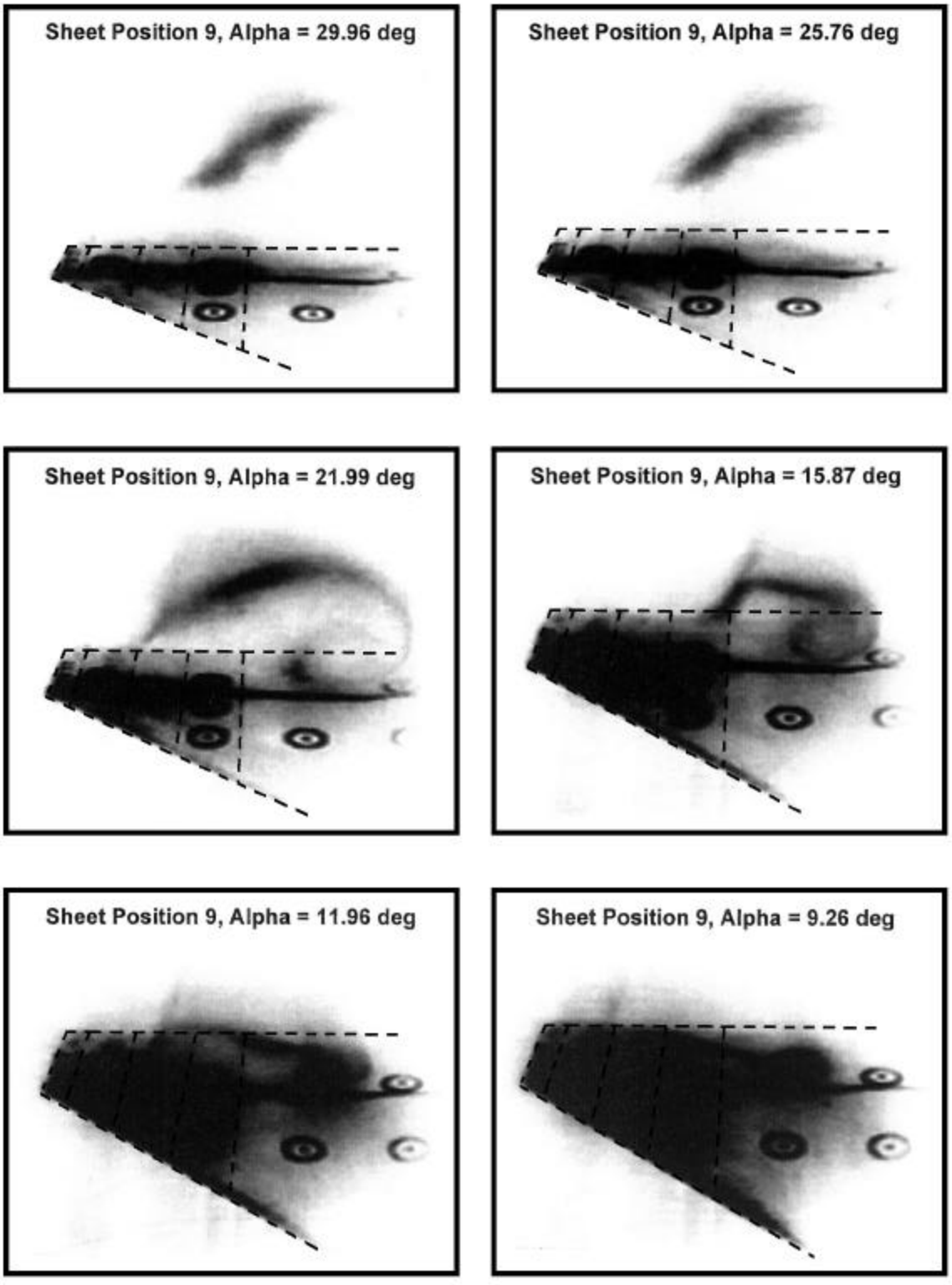

Figure 16: Unsteady Flow Visualization With the High-Speed CCD Camera: M = 0.9, Alpha = 34.97 deg – 9.01 deg, Pitch-Down

The transition to vortex flow on pitch-down is indicated in the dynamic normal force and pitching moment data in Figure 12 to occur at about 20 deg. The unsteady pressure data in Figure 14 at 16.24 deg are very similar to the steady data at 16.43 deg in Figure 8, and this agreement persists down to 12.3 deg as discussed in Reference 11. The unsteady flow-visualization image in Figure 16 at 15.87 deg is likewise very similar to that for steady flow in Figure 9 at 16.43 deg. The transition to vortex flow from shocklet/finger-vortex flow occurs at 18.5 deg for pitch-down as also was discussed in Reference 11. This is very similar to the steady transition angle and correlates with the merging of the steady and unsteady normal force curves in Figure 12.

The final phase of pitch-down flow development involves transitions to leading edge flow attachment on the outboard panel (to SITES) and to attached trailing edge flow (from SITES). Normal force and pitching moment data in Figure 12 show that there is hardly any distinction between pitch-down unsteady data and steady data. A comparison of pressure data for pitch-down in Figure 14 at 11.23 deg and 10.27 deg with steady data in Figure 8 at 11.39 deg and 10.39 deg shows that the flow conditions are quite different. This same observation is true for the comparison of flow-visualization data for pitch-down in Figure 16 at 11.96 deg and 9.26 deg and steady flow data in Figure 9 at 11.6 deg and 9.4 deg. Discussions in Reference 11 describe the transition points during pitch-down as occurring at about 9.5 deg for outer wing leading edge flow re-attachment and about 8.1 deg for transition from SITES. The latter transition is evident in the comparison of unsteady pressures in Figure 14 at 8.71 deg and steady pressures in Figure 8 at 8.39 deg and 10.39 deg. The inboard portion of the unsteady distribution is similar to that of the steady distribution at 8.39 deg, whereas the outboard portion of the unsteady data is more like the portion of the steady distribution at 10.39 deg (post-SITES). Thus, the lagging of flow transition angles on pitch-down is not generally consistent over the wing.

6.0 CONCLUSIONS

A flow-visualization test was conducted with the simple straked wing in August 1996 at the NLR, The Netherlands, for the purpose of obtaining flow-visualization data to complement the pressure and force database generated in a 1992 test of the same configuration. This test was conducted to examine the flow-field characteristics at high-alpha conditions that involve vortices, shocks, and separated flows. Laser light sheet/water vapor techniques were used to illuminate the flows, and video recording was used to obtain the data. Both low- and high-speed video cameras were used to examine spanwise and streamwise laser sheet positions. In addition, under NLR funding, some preliminary particle image velocimetry (PIV) data were obtained at M = 0.225 and 0.6, as well as some pulsed laser flow visualization (9 nano-sec pulse) at M = 0.9.

At M = 0.9, the many complexities of transonic vortex flows were explored. Between high-speed video recordings at multiple positions and conventional video data at other positions, streamwise and spanwise flow characteristics were identified. This database was augmented by the force and pressure data obtained during the test in 1992. Both spatial and temporal details were obtained of the complex interactions of primary vortices, turbulent shear layers, stalled regions, and shocks where, for example, a normal shock was observed in the core of the strake vortex. The wing vortex at transonic speeds was found to be a more diffused region of shear layers and shocks rather than the well-formed vortex seen at low speeds. The flow-field regimes addressed were (1) attached transonic flow, (2) shock-induced trailing edge separation (SITES) and tip leading edge separation, (3) transonic vortex flow, (4) shocklets and finger vortices, and (5) turbulent separation boundary during progressive stalling.

Unsteady effects were also addressed at M = 0.9 where the lagging was highlighted for various flow features in the five flow regimes identified for steady flow. In general, the expected trends were observed in pressure, force, and flow-visualization data. On pitching-up, steady flow characteristics were seen to exist at higher angles dynamically. On pitching-down, these same features were seen to exist dynamically at lower angles than for steady flow.

The database contained in References 11, 12 and 13 has been included in the RTO database for Verification and Validation Data for Computational Unsteady Aerodynamics (Reference 16).

7.0 ACKNOWLEDGEMENTS

The force and pressure testing was conducted in April/May 1992 at the NLR under Air Force Contact F33657-84-C-0247 (CCP 4551) for the Aeronautical Systems Center, Wright-Patterson Air Force Base, Ohio, and was administered by Mr. F. Zapata of the F-16 SPO and Mr. L. J. Huttsell (AFRL/VASV). The flow-visualization testing was conducted in August 1996 under Air Force Contract F49620-94-C-0093 for the Air Force Office of Scientific Research, Bolling Air Force Base, DC, and administered by Dr. L. Sakell, AFOSR/NA. Funding was provided by the Wright Laboratory Flight Dynamics Directorate, Wright-Patterson Air Force Base, Ohio, and administered by Mr. L. J. Huttsell (AFRL/VASV). Additional funding was provided by NLR and by the Dutch Ministry of Defense, for which the monitors were Mr. C. Hoffman and Mr. E. Bos of the Netherlands Agency for Aerospace Programs (NIVR Contract: 07501N).

8.0 REFERENCES

1. Cunningham, A. M., Jr.; den Boer, R. G., et al.: Unsteady Low-Speed Wind Tunnel Test of a Straked Delta Wing, Oscillating in Pitch; AFWAL-TR-87-3098 (Parts I through VI), April 1988.

2. den Boer, R. G. and Cunningham, A. M., Jr.: "Low-speed Unsteady Aerodynamics of a Pitching Straked Wing at High Incidence - Part I: Test Program," Journal of Aircraft, Vol. 27, January 1990, pp. 23-30.

3. Cunningham, A. M., Jr. and den Boer, R. G.: "Low-speed Unsteady Aerodynamics of a Pitching Straked Wing at High Incidence - Part II: Harmonic Analysis," Journal of Aircraft, Vol. 27, January 1990, pp. 31-41.

4. Cunningham, A. M., Jr.: "A Critique of the Experimental Aerodynamic Data Base for an Oscillating Straked Wing at High Angles," Proceedings Fourth Symposium on Numerical and Physical Aspects of Aerodynamic Flows, California State University, Long Beach, California, 16-19 January 1989.

5. Cunningham, A. M., Jr. and den Boer, R. G.: "Steady and Unsteady Aerodynamics of a Pitching Straked Wing Model at High Angles of Attack," presented at the AGARD FDP Symposium "Vortex Flow Aerodynamics," Scheveningen, Netherlands, 1-4 October 1990.

6. Cunningham, A. M., Jr. and den Boer, R. G.: "Analysis of Unsteady Force, Pressure and Flow-Visualization Data for a Pitching Straked Wing Model at High Angles of Attack," presented at the AGARD FDP Specialists' Meeting "Maneuvering Aerodynamics," Toulouse, France, 1-2 May 1991.

7. den Boer, R. G. and Cunningham, A. M., Jr.: "Unsteady Transonic Wind Tunnel Testing of Fighter Type Wings," 31st AIAA/ASME/ASCE/AHS/ASC Structures, Structural Dynamics, and Materials Conference, Long Beach, California, 2-4 April 1990.

8. Cunningham, A. M., Jr. and den Boer, R. G.: Overview of Unsteady Transonic Wind Tunnel Test on a Semi-Span Straked Delta Wing Oscillating in Pitch, WL-TR-94-3017, WL-TR-94-3095, and WL-TR-94-3096, August 1994.

9. Cunningham, A. M., Jr.: "A Preliminary Assessment of the Transonic Aerodynamic Characteristics of a Straked Wing Configuration," Lockheed Martin Tactical Aircraft Systems, Fort Worth, TX, July 1993.

10. Cunningham, A. M., Jr.; Geurts, E. G. M.; Dogger, C. S. G.; and Persoon, A.J.: Transonic Wind Tunnel Test on the Flow-Visualization of a Semi-Span Simple Straked Delta Wing Model, National Aerospace Laboratory, Netherlands, Contract Report, CR97577L (Parts I and II), January 1998.

11. Cunningham, A.M., Jr. and Geurts, E. G. M.: Analysis of Limit Cycle Oscillation/Transonic High Alpha Flow Visualization, Part 1: Discussion, AFRL-VA-WP-TR-1988-3003, January 1998.

12. Cunningham, A. M., Jr.; Geurts, E. G. M.: Analysis of Limit Cycle Oscillation/Transonic High Alpha Flow Visualization, Part 2: Stationary Model Data, AFRL-VA-WP-TR-1998-3004, January 1998.

13. Cunningham, A. M., Jr.; Geurts, E. G. M.: Analysis of Limit Cycle Oscillation/Transonic High Alpha Flow Visualization, Part 3: Oscillating Model Data, AFRL-VA-WP-TR-1998-3005, January 1998.

14. Geurts, E. G. M. and Cunningham, A. M., Jr.: Flow Visualization and Particle Image Velocimetry on a Semi-Span Straked Delta Wing, Stationary and Oscillating in Pitch, National Aerospace Laboratory, Netherlands, Report TP97261L, 1997.

15. Campbell, J. F. and Chambers, J. R.: Patterns in the Sky - Natural Visualization of Aircraft Flow Fields. NASA SP-514, 1994.

16. Verification and Validation Data for Computational Unsteady Aerodynamics, RTO-TR-26, AC/323(AVT) TP/19, NATO, October 2000.